Diagenetic and Detrital Origin of Moretane Anomalies through the Permian-Triassic Boundary

Comment [KF1]: The title was changed to reflect to modification of our argument

Authors:

French, Katherine L.[a]

Tosca, Nicholas J.[b]

Cao, Changqun[c]

Summons, Roger E.[d]

Affiliations:

a. Joint Program in Chemical Oceanography, Massachusetts Institute of Technology and Woods Hole Oceanographic Institution, Cambridge, Ma 02139, United States
b. Department of Earth Sciences, University of St Andrews, St Andrews, KY16 9AL, Scotland UK
c. State Key Laboratory of Palaeobiology and Stratigraphy, Nanjing Institute of Geology and Palaeontology, Chinese Academy of Sciences, Nanjing, Jiansu, 210008, China
d. Department of Earth, Atmospheric, and Planetary Sciences, Massachusetts Institute of Technology, Cambridge, Ma 02139, United States

Key words: Late Permian Extinction; Meishan Section; hydrocarbon biomarkers; hopanes; moretanes; clay composition; diagenesis; berthierine

ABSTRACT

Many biogeochemical anomalies coincide with the Late Permian Extinction (LPE; 252.28 Ma). Several mechanisms have been proposed to explain the moretane/hopane anomaly that has been identified in samples from Meishan GSSP section in southeastern China. Here, we report homohopane, 2α- and 3β-methylhomohopane and lithological data for a drill core from the Meishan section in southeastern China. Three intervals of elevated C_{30} moretane/hopane ratios are recorded in the Lungtan, Yinkeng and Helongshan Formations. Moretane/hopane ratios of C_{31-34} homohopanes and the 2α- and 3β-methylhomohopanes display the same stratigraphic patterns as the C_{30} moretane/hopane record. In light of the multiple and parallel moretane anomalies for the homohopane and 2α- and 3β-methylhomohopane series, enhanced input from higher plant organic matter, such as coal and peat, does not adequately explain the observed isomer patterns. Correlation of high moretane/hopane ratios with low C_{35} HHI and high hopane/sterane values suggest increased input of hopanoids from oxic soils. Additionally, moretane/hopane ratios show excellent correlations with total clay percentages and specific clay types, particularly chlorite, illite, and mixed layer illite/smectite. We conclude that a combination of episodic hopanoid input from soil bacteria and diagenetic effects related to redox and detrital clays generated the unique moretane/hopane patterns at Meishan.

Similar relationships of Ts/(Ts+Tm) with redox and source indicators and lithology indicate that Ts/(Ts+Tm) is affected by the same factors controlling the

Comment [KF2]: Rewrote because of Simon's comment about word choice in this sentence

moretane/hopane ratios. Berthierine, a clay that requires reducing conditions for formation, was detected in samples from the Lungtan Formation. We are unable to determine from our results whether the berthierine is authigenic or detrital, but future determination of the origin of berthierine at Meishan may offer additional environmental insight. No link between diasteranes and lithology was observed in this study suggesting that diasteranes are relatively unaffected by the detrital clay component of the Meishan sediments. In total, the results point toward the complex role of source input, lithology, and depositional redox conditions in the transformation of organic matter during maturation. Future work is required to elucidate the lithological effects on diagenetic processes, including biomarker genesis isomerization, and thermal degradation.

Comment [KF3]: Expanded and added more detail to the end of the abstract as Simon suggested. I removed some of the broad generatlizations that were originally at the end of this section.

INTRODUCTION

Through the course of Earth's 4.5 billion year history, there have been five mass extinction events in which at least 75% of species became extinct in a geologically short time interval. Given the rapid loss of biodiversity over the past centuries, some researchers have suggested that Earth may currently be entering its sixth mass extinction event (Barnosky et al., 2011). Humans are suspected to have a role in today's loss of biodiversity, but other conditions and series of events must have caused the previous five mass extinctions. The Late Permian Extinction (LPE; 252.28 Ma) (S. Shen et al., 2011), which occurred shortly before the biostratigraphic Permian Triassic Boundary (PTB) as defined by the first appearance of *Hindeodus parvus*, marks the greatest loss of biodiversity in Earth history with over 90% of marine species becoming extinct (Raup, 1979; Mundil et al., 2001, 2004; Sepkoski, 2002; Erwin, 2006; Metcalfe and Isozaki, 2009). Many mechanisms have been proposed to trigger the LPE event, including Siberian flood basalt volcanism, sea level change, extraterrestrial impact, ocean deoxygenation, water column stratification and climate change driven by methane hydrate collapse (Campbell et al., 1992; Wignall and Hallam, 1992; Renne et al., 1995; Becker et al., 2001; Benton and Twitchett, 2003; Kamo et al., 2003). Whatever the trigger or combination of triggers, accumulating evidence points to the rapid deterioration of both the marine and terrigenous ecosystems (Retallack, 1995; Looy et al., 2001; Twitchett et al., 2001; Michaelsen, 2002).

Comment [KF4]: This edit was made in hopes of clarifying Ken's questions about the boundary

Geochemical techniques have helped to elucidate the nature of the events that unfolded during the Late Permian, yet additional questions have arisen as a result. In addition to a distinctive negative stable carbon isotopic excursion and trace metal enrichment at the boundary (Kaiho et al., 2001, 2006; Cao et al., 2002, 2009), anomalous distributions of lipid biomarkers, including isorenieratane and derived aryl isoprenoids, 2-methylhopanes and crocetane, are defining features of the PTB (Grice et al., 2005; Wang et al., 2005; Xie et al., 2005; Wang, 2007; Cao et al., 2009). Additionally, anomalous values of molecular ratios, including C_{30} 17β,21α(H)-hopane/C_{30} 17α, 21β(H)-hopane (referred to as the C_{30} moretane/hopane ratio), C_{27} 18α-trisnorhopane/C_{27} 17α-trisnorhopane (referred to as Ts/(Ts+Tm)), Tm/C_{30} hopane, C_{31}/C_{32} hopane, C_{35} Homohopane Index (C_{35} HHI), and hopane/sterane, are recorded in sediments deposited at the PTB (Wang, 2007; Xie et al., 2007; Cao et al., 2009).

Multiple scenarios have been proposed to explain the elevated moretane/hopane ratios at the PTB. Geochemical maturity parameters throughout the Meishan GSSP section in southeastern China are nearly uniform, and thus, thermal maturity variations cannot adequately explain the moretane/hopane and Ts/(Ts+Tm) variability observed through the section (Cao et al., 2009). Accordingly, additional mechanisms have been proposed to account for the moretane variability, including increased input of higher plant organic matter to the marine system, increased acidification, freshening of the upper water column, or lithological effects (Wang, 2007; Xie et al., 2007; Cao et al., 2009). In order to further assess and correctly interpret the moretane anomalies at the PTB, homohopane, 2α- and 3β-methylhomohopane and lithological data for a drill core taken from the

Meishan section in China were critically examined. The possible mechanisms for generating the observed moretane record, including thermal maturity, source input, redox conditions, and lithology, were examined in light of the new hopane and lithological data.

Comment [KF5]: Added redox to the list of factors we examined as suggested by Ken

1.2. Moretane Background

Hopanes are pentacyclic triterpanes and are arguably the most ubiquitous natural product found on Earth (Ourisson and Albrecht, 1992). Bacteria are the dominant source of hopanes in marine sediments, and bacteriohopanepolyols (BHP) are the primary precursor of C_{30} and higher hopane homologues. Hopanes have readily isomerized asymmetric carbon atoms at C-17 and C-21, where α and β denote whether the hydrogen is below or above the plane of the ring system, respectively. Consequently, when considering C-17 and C-21, there are four possible stereoisomers (Fig. 1): 17β,21β(H)-hopane (ββ-hopane), 17β,21α(H)-hopane (βα-moretane), 17α,21β(H)-hopane (αβ-hopane), and 17α,21α(H)-hopane (αα-hopane; this isomer is not generally encountered in sediments). The term "moretane" distinguishes the 17β,21α(H)-hopane stereoisomers from the other hopane stereoisomers, while the others are simply referred to as 'hopanes'. The ββ-hopanoids are the commonly observed biological configuration and are found in bacterial cultures and immature organic material. The ββ configuration is nearly planar, which enables the molecule to fit into the membrane lipid bilayer (Peters et al., 2005), but the ββ-hopane is the least thermodynamically stable of the hopane stereoisomeric series (Seifert and Moldowan, 1980; Kolaczkowska et al., 1990; Peters et al., 2005). During diagenesis and catagenesis, ββ-hopane is removed by thermal degradation or interconversion to the more thermodynamically stable βα-moretane and αβ-hopane.

According to the scheme illustrated in Seifert and Moldowan (1980), βα-moretane can overcome an energy barrier given sufficient thermal energy to be converted to the thermodynamically preferred αβ-hopane via the ββ-hopane intermediate (Peters et al., 2005). The αα-hopane is less thermodynamically stable than either 17β,21α(H)-moretane or 17α,21β(H)-hopane, and it is largely undetected in petroleum and mature petroleum source rocks (Bauer et al., 1983; Kolaczkowska et al., 1990).

The distributions of terpane isomers can be used to estimate thermal maturity. Predictions of thermodynamic stability of the different hopane stereoisomeric series and observations of the degree of isomerization of hopanes in immature organic matter and petroleum have led to use of the βα-moretane to αβ-hopane ratio as a thermal maturity indicator (Seifert and Moldowan, 1980; Peters et al., 2005). The βα-moretane/αβ-hopane ratio is used to characterize immature to mildly mature oils. However, thermal maturity is not the only factor that influences the βα-moretane/αβ-hopane ratio. The source of organic matter input and depositional environment influence the terpane fingerprint of petroleum and can significantly affect thermal maturity parameters (Peters et al., 2005). Based on reports of 17β,21α(H) hopanoids in hypersaline environments, peat, coal, lacustrine environments, and in living systems (Quirk et al., 1984; Rullkötter and Marzi, 1988; Uemura and Ishiwatari, 1995; Rosa‐Putra et al., 2001), some authors have invoked increased input of higher plant organic matter to explain anomalous moretane abundance in marine sediments where thermal maturity is not the cause of variability (Grantham, 1986; Isaksen and Bohacs, 1995; Wang, 2007; Xie et al., 2007). However, in a number of instances, depositional environment has been shown to strongly modulate

Comment [KF6]: Reworded in order to avoid confusion for igneous geochemists as pointed out by Simon. Seifert and Moldowan, 1980 was not specific about a temperature at which this conversion is expected to occur

Comment [KF7]: Simon had a comment abou the Chen et al., 2001 reference. It doesn't pertain to living systems. Wang, 2007 used Chen 2001 to argue for elevated moretanes in coaly strata although when looked again at the Chen paper the moretane data wasn't clearly presented, so I deleted this reference. It's inclusion in this list isn't required for our argument.

terpane distributions, including the abundance of moretane relative to αβ-hopane (Peters et al., 2005).

2. SAMPLES AND EXPERIMENTAL METHODS

2.1. Geographic Setting

The Meishan quarries in South China have produced detailed information about the Permian-Triassic mass extinction. The Meishan section is the Global Stratotype Section and Point (GSSP) for the PTB, as well as for the base of Changhsingian Stage. In order to avoid sampling material that was altered and contaminated during surficial weathering, a drilling project was undertaken by the Nanjing Institute of Geology and Paleontology in 2004. A detailed description of the Meishan section and the drilling project are provided in the supplementary online material of Cao et al. (2009).

2.2. Biomarker Analyses

As described by Cao et al. (2009), the exterior of the samples were brushed clean and rinsed with methanol (MeOH) and dichloromethane (DCM) prior to being powdered using a solvent-cleaned ceramic puck mill. Procedural blanks were prepared along with the samples and showed no evidence of laboratory contamination. Samples were solvent extracted using a Dionex ASE-200 extractor and a solvent mixture of DCM and MeOH (9:1). Elemental sulfur was removed from the total lipid extracts using acid-washed copper granules. Aliphatic, aromatic, and polar fractions were collected by silica column chromatography using hexane, hexane/DCM (4:1), and DCM/MeOH (4:1) solvents, respectively.

Each fraction was dried and weighed before adding analytical standards to 1 mg of the saturated fraction. The saturated hydrocarbon biomarkers were analyzed by gas chromatography-mass spectrometry (GC-MS) in full scan and metastable reaction monitoring (MRM) modes. The characteristic *m/z* 191 and 205 mass fragments were used to identify the C_{30}-C_{34} homohopanes and 2α- and 3β- methylhopanes in MRM mode, respectively (see Fig. 2). The 22S and 22R isomers of $C_{31\text{-}34}$ homohopanes and $C_{32\text{-}33}$ methylhomohopanes were identified, and both isomers were used in the calculation of the βα/(βα + αβ) ratios. The 22S and 22R isomers of βα-C_{31} homohopane and βα-C_{32} methylhomohopane coelute, so these compounds were integrated as a single peak as illustrated in figure 2. The supplementary online material of Cao et al. (2009) describes the biomarker analytical methods in greater detail.

Comment [KF8]: Simon had a question about whether both the S and R isomers were integrated and used in calculation and whether MRM or SIM data was used for calculation. This concern about calculation of the moretane/hopane ratio and mode of analysis is addressed and clarified here.

The labeling of the 22S and 22R isomers of βα-C_{31} homohopane and βα-C_{32} methylhomohopane in figure 2 was edited to reflect that the two isomer peaks coelute for these two compounds. This should also address another question Simon had about how the chromatograms were originally labeled.

2.3 Mineralogical Analyses

2.3.1 Carbonate Contents

Approximately 0.5 g of each powdered sample was accurately weighed into a clean Teflon tube. Methanol was added to wet the sample prior to acidification. Each sample was acidified with a 10% aqueous hydrochloric acid (HCl) solution. The samples were treated again with a 15% HCl solution and left for 24 hours to allow the reaction to reach completion. The samples were rinsed with water five times to remove any remaining acid before being dried in a 60°C oven for 48 hours. The samples were reweighed, and the percentage carbonate was calculated based on the difference between the initial and final weights.

172

173 *2.3.2 Clay analyses*

174 Preparation for bulk mineralogical analysis of all samples involved crushing rock
175 samples in an agate swing mill, addition of 10 wt. % ZnO and further milling to ensure
176 mixing and homogeneous distribution. Bulk mineralogical analysis was performed on
177 randomly oriented samples using a Bruker D8 X-ray diffractometer at 40 kV and 30 mA
178 with CuKα radiation. Analyses were performed from 2-65° 2Θ (for any diffracted X-ray
179 obeying Bragg's Law, 2Θ as referred to herein is equal to 2 times the angle between the
180 sample plane and the incident X-ray beam) at a step size of 0.02 degrees and counting
181 times of 4 seconds per step. Quantitative analysis was performed with single line and full
182 profile fitting using pure mineral standards for reference intensity ratios (Srodon et al.,
183 2001).

184

185 Determination of clay mineralogy involved light crushing of samples by hand in a
186 steel mortar and pestle and for samples containing appreciable carbonate content,
187 decarbonation with 1M acetic acid while monitoring pH. Decarbonated samples were
188 rinsed three times with deionised water and all samples were resuspended with sodium
189 phosphate, sonicated and the <2 and <0.2 μm size fractions were obtained by timed
190 centrifugation. Centrifuged samples were decanted and oriented Ca-saturated aggregates
191 were prepared by using a filter membrane technique and transfer of clay films for glass
192 substrates. X-ray diffraction was performed using a Siemens D5000 diffractometer at
193 30kV and 20 mA, with CuKα radiation from 2-35° 2Θ a step size of 0.03 degrees and
194 counting times of 8-10 seconds. Divergence, receiving and anti-scatter slits were 0.2 and

Comment [KF9]: This section was added to clarify a question Ken had in his hand-written edits

1 mm in size, respectively, and a Ni filter was used. Clay samples were analysed in the air-dried Ca-saturated state, after ethylene glycol solvation overnight at 60^{o}C (to identify expandable minerals), heating at 400^{o}C for 2 hours (to quantify collapsible/expanding mineral proportions), and heating to 550^{o}C for 2 hours (to aid in quantifying kaolinite and chlorite proportions). Relative clay abundances were determined by peak area measurement, expressed in relative percent and normalized to total clay content by total clay mineral abundance determined by bulk mineralogical analyses. The composition of mixed-layered species was determined using one dimensional X-ray diffraction pattern modeling with the software package NEWMOD (Reynolds and Reynolds, 1996).

3. RESULTS

3.1 Stratigraphic Variation of Lithology and Hopane Distributions

The βα/(βα + αβ) ratios for C_{30} hopane, $C_{31\text{-}34}$ homohopanes, $C_{31\text{-}33}$ 2α-methylhopanes, and $C_{31\text{-}33}$ 3β-methylhopanes were calculated for each sample (Table 1). The precise determination of βα/(βα + αβ) for the C_{31} and C_{32} 3β-methylhopanes was precluded by interfering peaks and will not be further discussed. The βα/(αβ+βα) values vary from 0.04 to 0.34 for all of the other hopane series measured. The profiles of C_{30} hopane, the homohopanes, and the 2α- and 3β-methylhomohopanes show parallel downcore trends and similar values (Fig. 3). Ts/(Ts+Tm) and C_{35} Homohopane Index (HHI) data from Cao et al., 2009 were plotted in figure 3 for comparison. Notably, the rocks record three positive moretane enrichments. The first interval of enhanced moretane/hopane ratios occurs in the Lungtan Formation, followed by the second interval at the PTB in the Yinkeng Formation, and the last interval of moretane enrichment at the end of the Griesbachian in the Helongshan Formation.

Comment [KF10]: The sentence about interference from gammacerane was removed according to Simon's comment. We agree that it is unlikely that gammacerane causes the slight elevation of C31 homohopane over the other homohopanes. This was an error. However, this minor observation isn't central to our argument.

Comment [KF11]: The error of naming only 2 of the three anomalies was fixed here and in the other places

The bulk lithology, including percent carbonate, total clay, and quartz was determined (Table 2). The lithology was highly variable through the drill core section (Fig. 4). The percent carbonate fluctuates from 8.5 to 99%. The percent total clay and the percent quartz both vary from close to 0% to nearly 50%. The Lungtan Formation is a clay-rich unit that is enriched in quartz and is characterized by low carbonate (8.5 to 14%). The percent carbonate increases significantly in the overlying Changxing unit, although the carbonate and quartz percentages are more variable through this interval.

Unlike the Lungtan Formation, clay is a minor component through the Changxing Formation. The percent total clay returns to elevated values in the Yinkeng Formation, while the percent carbonate is significantly lower than the Changxing or Helongshan formations. Through the Helongshan Formation, the samples are all over 95% carbonate with very little clay or quartz. Like as also found by Rullkötter and Marzi (1988), elevated abundances of moretanes relative to αβ-hopane are associated with carbonate-poor facies.

Further clay mineralogical analyses provided the absolute and relative percentages of specific clay types, including illite, chlorite, smectite, kaolinite, berthierine, and mixed layer illite/smectite (Table 3). The total percent clay and the absolute and relative percentages of the clay type varied through the section (see Fig. 5). Illite and mixed layer illite/smectite represent the dominant clay types, where the sum of percent illite and mixed layer illite/smectite represents over 50% through the entire section. The relative percentage of illite/smectite mixed layer clay is largely constant throughout the clay mineral assemblage. Although more variable, kaolinite, chlorite, and smectite clays become a significant fraction of the total clay through some intervals of the assemblage. Notably, berthierine, which is usually formed under reducing conditions (Taylor and Curtis, 1995; Fritz and Toth, 1997), is present in the Lungtan Formation at the base of the section. Measurable differences between the glycolated and heated (400 °C) samples in the 7 Å peak suggest that trace abundances of berthierine may be present in the samples between 92-103 m. It is not possible to determine from our results whether the berthierine is detrital or authigenic.

Comment [KF12]: We rechecked the samples in this interval according to Ken's suggestion.

Comment [KF13]: Unfortunatly, we can't distinguish whether the berthierine is detrital or authigenic, but this is an important consideration that we had not previously given enough weight. We address this in a later section specifically devoted to berthierine

253

254 **3.2 Crossplots of Molecular Indices and Lithological Data**

255 Cross-correlation diagrams were generated to evaluate the relationships between
256 the geochemical and lithological data. The βα/(αβ+βα) ratios of C_{30} hopane were plotted
257 against the βα/(αβ+βα) ratios of C_{31}-C_{34} homohopanes and the 2α and 3β-
258 methylhomohopanes (Fig. 6A and B). In both cases, an excellent positive correlation is
259 observed with R^2 values ranging from 0.88 to 0.99. Cao et al. (2009) found that
260 Ts/(Ts+Tm) varied inversely with the C_{30} hopane βα/(αβ+βα) ratio. Likewise, the
261 Ts/(Ts+Tm) data reported by Cao et al. (2009) also correlate inversely with the
262 homohopane and 2α- and 3β- methylhomohopane βα/(αβ+βα) ratios with R^2 values
263 ranging from 0.64 to 0.77 (Fig. 6C and D).

264

265 The carbonate percentage and total clay percentage were plotted against the
266 moretane/hopane ratios for all of the hopane series and Ts/(Ts+Tm) (Fig. 7). The percent
267 carbonate and percent clay have opposite relationships with the βα/(αβ+βα) ratios.
268 Carbonate percentage and the βα/(αβ+βα) ratios of all of the hopane series are inversely
269 related, having R^2 values ranging from 0.42 to 0.57. The correlation is significantly
270 improved with R^2 values from 0.74 to 0.87 when the βα/(αβ+βα) ratios are plotted against
271 total clay percentage. Similarly, the correlation of Ts/(Ts+Tm) with the total clay
272 percentage (R^2 = 0.52) is stronger than with the percent carbonate (R^2 = 0.36). However,
273 the R^2 values for Ts/(Ts+Tm) versus carbonate and total clay percentages are less than for
274 the βα/(αβ+βα) ratios in both cases.

275

The βα/(αβ+βα) ratios for all of the hopane series were plotted together with the percentages of the different clay types in Fig. 8. Like the total clay percentage, all of the clay types were directly related to βα/(αβ+βα), yet some clay types were more strongly correlated to βα/(αβ+βα) than others. Kaolinite had the weakest correlation with βα/(αβ+βα), having R^2 values from 0.024 to 0.222. Likewise, smectite was weakly correlated to βα/(αβ+βα), having R^2 values spanning 0.215 to 0.485. On the other hand, the percent chlorite was strongly correlated with βα/(αβ+βα), where R^2 values ranged from 0.773 to 0.901. Percent illite and percent mixed layer illite/smectite also yielded strong correlations with βα/(αβ+βα).

The Ts/(Ts+Tm) values from Cao et al. (2009) were plotted versus the different types of clays. Low values of Ts/(Ts+Tm) occur during intervals of high clay accumulation, in particular, intervals where chlorite, illite, and illite/smectite mixed layer clays comprise a higher proportion of rock lithology. The R^2 values for Ts/(Ts+Tm) were less than the R^2 values for the analogous βα/(αβ+βα) plots. Like βα/(αβ+βα), kaolinite and smectite produced the weakest correlation coefficients, while illite, chlorite, and mixed layer illite/chlorite had higher correlation coefficients with Ts/(Ts+Tm).

3.2 Crossplots of C_{35} Homohopane Index and Hopane/Sterane ratios with Moretane/Hopane, Ts/(Ts+Tm) and Lithological Data

The C_{35} HHI is a redox indicator, and redox conditions are known to affect the distribution of terpanes (Peters et al., 2005). Cross-correlation diagrams were generated to evaluate the relationships between C_{35} HHI data reported in Cao et al., 2009 and

Comment [KF14]: As a result of the comments concerning possible redox and detrital effects, we carefully reconsider redox and source input effects as indicated by C35 HHI and hopane/sterane ratios. These two suggestions led us to discover some new relationships that are described in this section

299 moretane/hopane ratios and Ts/(Ts+Tm) (Fig. 9). High moretane/hopane ratios for C_{30-34}
300 homohopanes and C_{31-33} methylhomohopanes correspond to low values of C_{35} HHI,
301 which are indicative of oxic conditions. On the other hand, low values of Ts/(Ts+Tm)
302 correspond with low values of C_{35} HHI. These results are consistent with previous results
303 relating redox indicators to moretane hopane ratios and Ts/(Ts+Tm) (Moldowan et al.,
304 1986; Rullkötter and Marzi, 1988; Wang, 2007). Interestingly, high values of
305 hopane/sterane percentages reported in Cao et al., 2009 correspond with high values of
306 moretane/hopane ratios for C_{30-34} homohopanes and C_{31-33} methylhomohopane and low
307 values of Ts/(Ts+Tm) (Fig. 9). This relationship is unexpected because if the abundance
308 of αβ-hopanes were driving the correlation between hopane/sterane ratios and
309 moretane/hopane ratios, one would expect an inverse pattern between these two
310 parameters, which is the opposite of what is observed.
311
312 The C_{35} HHI and hopane/sterane percentages were plotted against total clay
313 percent and all of the clay types detected in the Meishan section (Fig 10). In general, the
314 highest values of percent total clay and individual clay types correspond to C_{35} HHI
315 values less than 5%, but several samples with significant kaolinite abundances have
316 higher C_{35} HHI values. High values of hopane/sterane percentages are related to high
317 values of total clay, chlorite, illite, mixed layer illite/smectite (I/S), and smectite.
318 Kaolinite and berthierine do not display this same relationship with the hopane/sterane
319 percentages (see Fig. 10L and 10N).
320

Comment [KF15]: This is a new figure 9. The original figure 9 was removed according to Ken's suggestion, but we added two more figures given the new observations.

4. DISCUSSION

4.1 Possible Causes of Moretane Enrichment

The strong positive correlations between the C_{30} hopane βα/(αβ+βα) ratios and the homohopane and 2α- and 3β-methylhomohopane βα/(αβ+βα) ratios imply that the moretane/hopane ratios for all of the hopane series are controlled by the same mechanism, and the mechanism that caused the anomalously high moretane values is not confined or unique to the extinction horizon. Our results show that moretanes are enriched in rocks that are clay-rich and have C_{35} HHI values indicating oxic conditions, which is consistent with the results of Wang, (2007) and Rullkötter and Marzi, (1988). Thermal maturity, the source of organic matter and depositional environment are the three possible factors that can influence the distribution of triterpane isomers (Peters et al., 2005). One or more of these factors is likely responsible for generating the moretane excursions recorded in the Lungtan, Yinkeng and Helongshan formations.

Thermal maturity can be estimated by measuring the degree of isomerization, including the ratio of βα-moretanes to αβ-hopanes, the conversion of 22R to 22S for 17α, 21β(H)-homohopanes and the conversion of 20R to 20S steranes. The moretane to αβ-hopane ratio for the C_{30} compound declines with increasing thermal maturity from ~0.8 in immature rocks to <0.15 for mature rocks (Peters et al., 2005). While the ratio of moretanes to αβ-hopanes varies significantly through the drill core, the ratio of 22S/(22S+22R) for C_{31} homohopane is between 54 and 59% throughout the entire

Meishan drill core (Cao et al., 2009). According to Larcher et al. (1987), these values are expected for αβ-hopanes when the epimerization reaction that converts the biological 22R epimer to 22S has reached endpoint. The epimerization end point is met before the main phase of oil generation (Peters et al., 2005). The 20S/(20S+20R) ratios of the C_{27} steranes varies between 45-50%, which further supports the conclusion that the whole cored interval is within the early stages of petroleum generation and shows little variation throughout (Cao et al., 2009). The largely constant relative percent of illite/smectite mixed layer clay in the section is also consistent with constant thermal maturation throughout the Meishan drill core (Pollastro, 1993). Accordingly, thermal maturity can be ruled out as the factor responsible for moretane variability. Likewise, Wang (2007) and Xie et al. (2007) eliminated thermal maturity as a possible mechanism for generating the moretane anomaly based on additional lines of evidence.

The sources of organic matter profoundly affect biomarker distributions (Peters et al., 2005). Previous studies have argued that increased terrigenous organic matter input from higher plants, peat, or coal explains elevated moretane/hopane ratios in cases where thermal maturity does not sufficiently explain the pattern of moretane/hopane ratios (Grantham, 1986; Rullkötter and Marzi, 1988; Isaksen and Bohacs, 1995). The link between moretanes and higher plant organic matter input is based on a series of studies that detected elevated βα-hopanoids in terrigenous influenced sediments and some higher plants. Unusually high abundances of 17β(H), 21α- moretan-29-ol and 17β(H)-moret-22(29)-ene have been reported in acidic and saline lakes (Uemura and Ishiwatari, 1995; Ishiwatari et al., 2005; Aichner et al., 2010; Kristen et al., 2010). Quirk et al. (1984)

detected C_{32} βα-alcohols, C_{31} methylmoretan-29-ol, and C_{32} and C_{33} βα hopanoic acids in peat samples, and elevated levels of moretane were reported for coals (e.g., Hughes and Dzou, 1995; Shen and Huang, 2007). Second, although ββ-hopanes are the presumed biological isomer, βα-hopanoids have been identified in some organisms. The compounds 21α(H)-moret-22(29)-ene ($C_{30}H_{50}$) and 30-nor-21α-hopan-22-one (isoadiantone; $C_{29}H_{48}O$) were isolated from ferns and lichens (Hveding-Bergseth et al., 1983; Shiojima and Ageta, 1990; Tsuzuki et al., 2001). Moretenone and moretenol were isolated from a small shrub (Lavie et al., 1968), and Rosa-Putra et al. (2001) discovered that soil bacteria *Frankia spp*. synthesize 22(S)-moretan-29-ol ($C_{30}H_{52}OH$).

Based on the evidence discussed above, some researchers have argued that the PTB moretane anomaly signals increased organic matter input from higher plant material, particularly peat and coal (Wang, 2007; Xie et al., 2007). The data presented in this paper do not support this explanation. None of the previous reports linking higher plant organic matter input to elevated moretane abundances provide a viable explanation for the parallel trends of the extended homohopanes and the 2α- and 3β-methylhomohopanes because, with the exception of the peat samples reported by Quirk et al. (1984), the βα-hopanoids detected in organisms, peat, and coal are C_{29} or C_{30} compounds. Since thermal maturity and a change in input of higher plant organic matter fail to account for the observed moretane anomalies, other source input changes and diagenetic effects must be considered.

389 Redox potential is known to affect the distribution of terpanes in lipid extracts (Peters
390 et al., 2005). Multiple redox indicators are presented for the Meishan section in Cao et al.,
391 2009. Values of 28,30-dinorhopane (28,30-DNH) between 0.5 and 2% and the detection
392 of isorenieratane and C_{14-27} aryl isoprenoids throughout the cored interval indicates that
393 all of the sediments were deposited under reducing conditions. However, C_{35} HHI values
394 are highly variable through the drilled interval (0.10-14.47 %), which is inconsistent with
395 the multiple redox indicators that suggest reducing conditions throughout the cored
396 interval. Homohopane distribution depends on depositional redox conditions, sulfur
397 incorporation in organic matter, and biodegradation (Peters and Moldowan, 1991). The
398 rocks through the entire cored interval were deposited in a marine setting that likely had
399 the necessary sulfate concentrations required for homohopane distributions to reflect
400 redox conditions. The discrepancy of the C_{35} HHI with the other redox indicators and the
401 strong relationship of the C_{35} HHI with the moretane/hopane ratios, Ts/(Ts+Tm), and
402 lithological data suggest a detrital source for the clays and hopanes in the intervals of
403 elevated moretane/hopane ratios.
404
405 Multiple lines of evidence suggest increased soil erosion, forest fires, continental
406 weathering, and terrigenous input during the PTB (Ward et al., 2000; Retallack et al.,
407 1998, 2005; Sephton et al., 2005; Wang and Visscher, 2007; Cao et al., 2009; Nabbefeld
408 et al., 2010b; S. Shen et al., 2011; W. Shen et al., 2011). Although most studies do not
409 examine evidence earlier than the Changhsingian, detection of particular polycyclic
410 aromatic hydrocarbons (PAHs) in samples from Meishan prior to the extinction horizon
411 suggests that there may have been earlier pulses of land-derived organic matter to the

Comment [KF16]: Given the importance of redox as noted in Ken's review, we evaluated a number of redox indicators in relation to our data

412 marine system (Nabbefeld et al., 2010b). Interestingly, the highest values of retene, a
413 PAH thought to be derived from coniferous resin (Peters et al., 2005), is concurrent with
414 the earliest interval of moretane/hopane enrichment in the Lungtan Formation.
415 Accordingly, there may have been increased terrigenous input to the marine system
416 during the PTB and the Wuchiapingian, which is consistent with a detrital origin of clays
417 and hopanes during these intervals.
418
419 Increased organic matter input from higher plant matter cannot explain the parallel
420 patterns of βα/(αβ+βα) for C_{30-34} homohopanes and C_{31-33} methylhomohopanes, but
421 increased input of hopanoids from soil bacteria may explain the anomalous
422 moretane/hopane ratios observed in all hopane series. The hypothesis that there was an
423 influx of hopanoids from soil bacteria to the marine system is supported by the
424 observation that high moretane/hopane ratios for all hopane series are associated with
425 high hopane/sterane percentages. This hypothesis is further supported by the observation
426 that high hopane/sterane percentages are associated with high percentages of total clay
427 and high abundances of the clay types that are most tightly related to moretane/hopane
428 ratios (chlorite, illite, mixed layer illite/smectite, and smectite). We conclude that the
429 multiple intervals of elevated moretanes were characterized by increased input of
430 hopanoids derived from soils. However, this change in source input alone does not fully
431 explain the moretane stereochemical anomalies. While βα-hopanoids have been identified
432 in one type of soil bacteria (Rosa-Putra et al. 2001), it is more likely that the detrital clays
433 and redox conditions of the original depositional environment controlled the
434 stereochemistry of the soil-derived hopanoids that were ultimately deposited in marine

Comment [KF17]: In light of the suggestions about redox and detrital input, we evaluate the standing evidence for terrigenous input in relation to our data and observations

sediments. Therefore, a combination of hopanoid input from soils and diagenetic effects generated the unique moretane/hopanes patterns observed at Meishan.

Comment [KF18]: This section was added as a result of the added layer of complexity to our argument

4.2 Discussion of Possible Mechanisms for Mineral Preservation of βα-hopanoid Stereochemistry

Certain minerals are known to mediate diagenetic reactions. In addition to thermal maturity and the source of organic matter, depositional environment and lithology are known to affect the distribution of biomarkers, including the moretane/hopane ratio (Moldowan et al., 1986; Curiale and Odermatt, 1989; Peters et al., 2005). If given sufficient time and heat, the biological isomers decline relative to the thermodynamically preferred isomers. However, this simplistic view is further complicated by factors that affect the relative rates of hydrocarbon generation, isomerization, and thermal degradation (Lu et al., 1989; Farrimond et al., 1998). Mineral composition has been shown to affect the degree of isomerization for steranes and hopanes in natural systems as well as laboratory pyrolysis experiments (Rullkötter et al., 1985; Eglinton et al., 1986; Curiale and Odermatt, 1989; Lu et al., 1989; Peters et al., 1990; Farrimond et al., 1998; Pan et al., 2010), but distinguishing between mineral effects on biomarker genesis, isomerization, and thermal degradation is difficult. Moreover, it is possible that a combination of these mineral composition effects plays a role in controlling biomarker stereoisomer distribution.

Originally, it was believed that the biologically preferred ββ-hopane was converted to the βα-hopane and αβ-hopane according to the energy diagram and

458 schematic depicted in Seifert and Moldowan (1980). The thermodynamic stabilities of the
459 hopane stereoisomers were later confirmed by molecular mechanics (Kolaczkowska et
460 al., 1990); however, it was recognized that minerals could modulate the rates of
461 epimerization. In particular, acidic surface sites of certain clay types were shown to
462 catalyze isomerization, rearrangement, and hydrogen exchange reactions (Solomon and
463 Swift, 1967; Sieskind et al., 1979; Saxby et al., 1992). Alexander et al. (1984) proposed
464 an epimerization mechanism that proceeded through a planar sp^2 hybridized intermediate.
465 Due to the enhanced stabilities of tertiary, allylic, or benzylic carbocation and radical
466 intermediates, these positions interact with clay surface sites. The carbon adjacent to the
467 carbocation or radical intermediate then undergoes hydrogen exchange and loss of the
468 original stereochemistry if the hydrogen is added from the opposite face (Alexander et
469 al., 1984). If the mechanism proposed by Alexander et al. (1984) is correct, clay-
470 catalyzed epimerization may be stereoselective. In which case, the conversion of ββ-
471 hopane to αβ-hopane would be less favorable than the conversion to βα-hopane because
472 C_{22} is arguably the most accessible tertiary carbon in the hopane skeleton that could
473 interact with the clay surface and form a carbocation intermediate, thus promoting
474 epimerization at the adjacent C-21.
475
476 However, direct epimerization of the free ββ-hopane to βα-hopane and αβ-hopane
477 isomers is not the only factor that affects the isomeric distribution of hopanes. Indeed, the
478 rates of hydrocarbon release from kerogen and asphaltene, rates of generation of
479 hydrocarbons from functionalized moieties, and rates of hydrocarbon thermal degradation
480 may also play significant roles in controlling isomer distributions of biomarkers.

Mineralogy may mediate these processes, thus influencing the initial and final biomarker distribution (Eglinton et al., 1986; Huizinga et al., 1987; Larcher et al., 1988; Lu et al., 1989; Abbott et al., 1990; Bishop and Abbott, 1993; Bishop et al., 1998; Farrimond et al., 1998, 2002; Koopmans et al., 1998; Wei et al., 2006; Pan et al., 2009, 2010). Furthermore, both organic and inorganic protective matrices can affect lipid biomarker distributions (Hedges and Keil, 1995; Huang et al., 2008; Mead and Goni, 2008). Active clay surfaces, in particular, tend to selectively adsorb polar compounds (Pan et al., 2005). For this reason, the preservation and generation mechanisms of polar hopane precursor compounds may offer insight to the moretane anomalies at Meishan detailed in this report.

Hopanoic acids can be a significant source of free hopanes (Bennett and Abbott, 1999). Laboratory and field results have demonstrated that the degree of isomerization of free hopanes is greater than kerogen-bound and functionalized hopanoids, including hopanoic acids (Tannenbaum et al., 1986; Peters and Moldowan, 1991; Bishop et al., 1998; Murray et al., 1998; Farrimond et al., 2002; Lockhart et al., 2008). Isomerization in the hopane E-ring may occur during the decarboxylation of hopanoic acids to yield free hopanes or during bond cleavage of kerogen-bound hopanoids (Farrimond et al., 1998, 2002). Alternatively, rates of isomerization may be slower for bound hopanoids and functionalized hopanoids than for free hopanes, as discussed below.

Hopanoic acids released from kerogen or produced during early diagenesis may become adsorbed on the mineral matrix and/or polar organic matter by ionic interactions

(Huizinga et al., 1987; Thomas et al., 1993; Kubicki et al., 1999). Previous works show that "trapped" or "bound" hydrocarbons isomerize at slower rates than free hydrocarbons (Derenne et al., 1988; Jaffé and Gardinali, 1990; Jaffé et al., 1997). Likewise, adsorption of polar moretane precursors to the surface of a protective matrix could effectively retard the rates of isomerization until release at high maturities. Carboxylic acids tend to adsorb strongly on inorganic surfaces (Thomas et al., 1993). However, the preservation potential of the less mature hopanoic acid signature depends on the adsorptive capacity of the mineral surface (Ransom et al., 1998; Kubicki et al., 1999). The different surface chemistries associated with individual clay types have unique affinities for organic matter, which could explain the different correlation strengths observed for βα/(αβ+βα) and the different clay types at Meishan. However, a more comprehensive study is required that characterizes the interaction of polar precursors of hopanoids with the clay types at Meishan and monitors hopanoic acid interactions with the mineral surface over a range of temperature and times.

4.3 Discussion of Depositional Environment, Source Input, and Ts/(Ts+Tm)

Like the moretane/hopane ratios, the Ts/(Ts+Tm) thermal maturity parameter is also strongly influenced by source input, lithology, oxicity, and acidity of depositional environment (McKirdy et al., 1983; Moldowan et al., 1986; Waples and Machihara, 1990; Dahl et al., 1993; Peters et al., 2005; Bennett and Olsen, 2007). According to molecular mechanics and observation, Tm (or C_{27} 17α-trisnorhopane) is less stable than the rearranged Ts isomer (or C_{27} 18α-trisnorhopane) (Seifert and Moldowan, 1978; Kolaczkowska et al., 1990). According to Fig. 6, Ts/(Ts+Tm) seems to be related not

only to C_{30} βα/(αβ+βα) as shown in Cao et al. (2009), but it is also inversely related to the βα/(αβ+βα) values of the homohopane and 2α- and 3β- methylhomohopane series. This inverse relationship would be expected for Ts/(Ts+Tm) and βα/(αβ+βα) if thermal maturity was the primary control on these parameters. Like βα/(αβ+βα), Ts/(Ts+Tm) co-varies with total clay percent, specific clay type abundances, C_{35} HHI, and hopane/sterane percentages at the Meishan section. As discussed above, maturity parameters that more appropriately evaluate the thermal history of this section, indicate relatively constant thermal maturity through the section, so the same mechanisms that are influencing the moretane/hopane ratios are likely affecting Ts/(Ts+Tm). Unlike previous studies that show that carbonate source rocks tend to generate oil with lower Ts/(Ts+Tm) values than clay-rich source rocks (McKirdy et al., 1983; Waples and Machihara, 1990; Peters et al., 2005; Bennett and Olsen, 2007), our results show that low values of Ts/(Ts+Tm) coincide with intervals of high clay content. However, our results are consistent with previous work that indicates Tm is favored over the rearranged, more stable isomer Ts in oxidizing conditions (Moldowan et al., 1986). Like our results that show high values of Ts/(Ts+Tm) in carbonate-rich rocks deposited under reducing conditions, Rullkötter and Marzi, (1988) found higher values of Ts/(Ts+Tm) associated with the relatively carbonate-rich Lias ε unit which was deposited under reducing conditions compared to the adjacent carbonate-poor mudstone facies that was deposited under oxic conditions. Input of soil-derived hopanoids seems to play a role in the moretane/hopane ratio patterns, and the relationship of Ts/(Ts+Tm) with hopane/sterane percentages suggests that source input may be affecting Ts/(Ts+Tm) as well. In total, these results indicate that a combination of source input effects and depositional factors,

including oxicity and lithology, control Ts/(Ts+Tm) and complicate the interpretation of this geochemical indicator.

4.4 Discussion of Lithology, C_{35} Homohopane Index and Additional Molecular Parameters

Lithology and redox conditions affect other molecular maturity parameters in addition to moretane/hopane ratios and Ts/(Ts+Tm) (Peters et al., 2005). Molecular parameters from Cao et al. (2009), including 28,30-bisnorhopane/C_{30} hopane, gammacerane/C_{30} hopane, C_{29} diasterane/regular sterane, and C_{27} diasterane/regular sterane were plotted against percent carbonate, percent total clay, percent total clay/TOC, C_{35} HHI, and hopane/sterane percentages. No significant correlations were identified with the exception of an inverse correlation of C_{29} diasterane/regular sterane and C_{27} diasterane/regular sterane with hopane/sterane percentages. The absence of any relationship with clay/TOC is counter to the results of van Kaam-Peters et al. (1998) and Nabbefeld et al. (2010a), although the different environmental settings, lithologies, and methods may partially explain the discrepancy.

Having recognized a detrital, clay-borne contribution to the hopanoid inventory during intervals of enhanced moretane accumulation at Meishan, the absence of a relationship between diasterane/regular sterane ratio and lithology comes into focus. Terrigenous organic matter tends to have higher abundances of hopanoids and lower contents of steroids relative to TOC compared to marine organic matter (Peters et al., 2005; Handley et al., 2010; Sáenz et al., 2011). Thus, in marine settings the sources of steroids are mainly marine algae from the water column. During sedimentation in a

Comment [KF19]: We drew this distinction according to Simon's comment

strongly reducing setting, steroids may be relatively unaffected by diagenetic processes associated with the clays. In other words, in this particular environment steroid and hopanoid diagenetic processes are decoupled to the degree that some fraction of the hopanoids is derived from detrital sources while the sterols are predominantly of local origin.

4.5 Potential Sources of Berthierine

The discovery of measurable berthierine and evidence of trace berthierine in the Lungtan and Yinkeng Formations, respectively, is an observation with multiple possible environmental implications. Berthierine forms in reducing environments, but low levels of sulfide and bicarbonate are also required because pyrite or siderite formation is favored over berthierine formation in reducing conditions in the presence of sulfide and bicarbonate, respectively (Taylor and Curtis; 1995; Fritz and Toth, 1997; Sheldon and Retallack, 2002). Interestingly, the berthierine-rich samples occur in the only kaolinite-rich interval of the section, and kaolinite is implicated in the formation of berthierine (Sheldon and Retallack, 2002). In contrast, samples from the Yinkeng Formation with evidence of trace berthierine are kaolinite-poor and smectite-rich. Smectite and kaolinite signify different weathering conditions, and as a result, the clay composition of these two intervals indicates that two different soil types are contributing to the sediments.

The detection of berthierine in samples from the Lungtan Formation where low C_{35} HHI values indicates oxic conditions suggests that one or both of these redox indicators have a detrital component. While it is not possible to conclusively determine from our results whether the berthierine is authigenic or detrital, it is interesting to note

Comment [KF20]: We were able to add more detail about the possible reason for an absence of this relationship given our modified interpretation or our data. This section should also satisfy Simon's request to expand upon the lack of relationship between diasteranes and lithology

Comment [KF21]: This section was added because we had not previously considered the Sheldon and Retallack reference or whether the berthierine was authigenic or detrital. We agree that these are both important points

596 that berthierine was discovered in high latitude paleosols deposited in the Early Triassic
597 following the PTB (Sheldon and Retallack, 2002). Formation of berthierine in soils is
598 rare because of the environmental requirements for formation, but weathering or erosion
599 of berthierine-containing paleosols could contribute detrital berthierine to the marine
600 setting. The berthierine-containing paleosols reported in Sheldon and Retallack, 2002 do
601 not correspond well spatially or temporally with the berthierine-rich samples in the
602 Lungtan Formation, but the discovery of berthierine in paleosols may offer a possible
603 mechanism for delivery of berthierine to marine sediments in the event that the
604 berthierine is detrital.
605
606

5. CONCLUSIONS

Comment [KF22]: This section was edited to reflect our modified interpretation

Three periods of moretane enhancement, two in the Triassic and one in the Permian, are recorded in the core from the Meishan section in southeastern China. These C_{30} moretane/hopane excursions are echoed in the homohopanes and 2α- and 3β-methylhomohopanes. In light of the multiple and parallel moretane 'anomalies' for the homohopane and 2α- and 3β-methylhomohopane series, enhanced input from higher plant organic matter does not adequately explain the observed hopane isomer patterns at Meishan. Correlation of high moretane/hopane ratios with low C_{35} HHI and high hopane/sterane ratios suggest increased input of hopanoids from soils that are influenced by oxic conditions during transport. However, this shift in source input alone cannot explain the hopane stereochemical patterns at Meishan. Based on C_{35} HHI and mineralogical analyses, it is concluded that diagenetic processes related to lithology and redox determine the βα-moretane/αβ-hopane distribution for all of the hopane series throughout the cored interval. It seems likely that certain clay types preferentially bind triterpanes having the moretane configuration. Berthierine, a clay that is formed in reducing conditions, was detected in samples from the Lungtan Formation. It is unclear from our results whether the berthierine is authigenic of detrital, but future determination of the origin of berthierine at Meishan may offer additional environmental insight.

Additional molecular parameters were tested for relationships with lithology. Hopane/sterane ratios, C_{35} HHI, percent total clay, chlorite, illite, and illite/smectite mixed layer clay showed significant relationships with Ts/(Ts+Tm), suggesting source input, lithology, and redox also affect this ratio. However, unlike previous studies (van

630 Kaam-Peters et al., 1998; Nabbefeld et al., 2010a) that reported a link between
631 diasteranes and percent clay/TOC, this relationship was noticeably absent in the
632 sediments at Meishan. Therefore, it seems likely that the diagenesis of steroids here was
633 decoupled from the clay component and more under the control of the intense reducing
634 conditions that prevailed in the water column. In total, our results point toward a complex
635 role of redox and lithology in the transformation of organic matter during diagenesis and
636 maturation. Future work is required to disentangle the lithological effects on diagenetic
637 processes, including biomarker genesis isomerization, and thermal degradation. We
638 conclude that a combination of episodic hopanoid input from soil bacteria and diagenetic
639 effects related to redox and detrital clays generated the distinctive moretane/hopane
640 patterns at Meishan.
641
642 *Acknowledgments*. We wish to thank Christian Hallman and Jürgen Rullkötter for
643 discussions and constructive suggestions, and Bob Burruss, Simon George, and Ken
644 Peters for informative reviews and insightful comments that strengthened this work.
645 KLF is supported by a National Science Foundation Graduate Fellowship. Research at
646 MIT was supported by an award (NNX09AM88G) from the NASA Exobiology Program
647 to RES. Research at Nanjing was supported by the 973 Project of the MST of China
648 (2011CB808905) and NSF of China. NJT acknowledges support from Churchill College
649 and the Royal Society (RG 2009/R2).
650

References

Abbott G., Wang G., Eglinton T., Home A., Petch G., 1990. The kinetics of sterane biological marker release and degradation processes during the hydrous pyrolysis of vitrinite kerogen. *Geochim. Cosmochim. Acta* **54**, 2451-2461.

Aichner B., Wilkes H., Herzschuh U., Mischke S., Zhang C., 2010. Biomarker and compound-specific $\delta^{13}C$ evidence for changing environmental conditions and carbon limitation at Lake Koucha, eastern Tibetan Plateau. *J. Paleolimnol.* **43**, 873-899.

Alexander R., Kagi R., Larcher A., 1984. Clay catalysis of alkyl hydrogen exchange reactions--reaction mechanisms. *Org. Geochem.* **6**, 755-760.

Barnosky A.D., Matzke N., Tomiya S., Wogan G.O.U., Swartz B., Quental T.B., Marshall C., Mcguire J.L., Lindsey E.L., Maguire K.C., Mersey B., Ferrer E.A., 2011. Has the Earth's sixth mass extinction already arrived? *Nature* **470**, 51-57.

Bauer P., Dunlap N., Arseniyadis S., Watt D., Seifert W., Moldowan J., 1983. Synthesis of biological markers in fossil fuels. 1. 17α and 17β isomers of 30-norhopane and 30-normoretane. *J. Org. Chem.* **48**, 4493-4497.

Becker L., Poreda R., Hunt A., Bunch T., Rampino M., 2001. Impact event at the Permian-Triassic boundary: evidence from extraterrestrial noble gases in fullerenes. *Science* **291**, 1530-1533.

Bennett B., Abbott G., 1999. A natural pyrolysis experiment - hopanes from hopanoic acids? *Org. Geochem.* **30**, 1509-1516.

672 Bennett B., Olsen S.D., 2007. The influence of source depositional conditions on the hydrocarbon
673 and nitrogen compounds in petroleum from central Montana, USA. *Org. Geochem.* **38**,
674 935-956.

675 Benton M., Twitchett R., 2003. How to kill (almost) all life: the end-Permian extinction event.
676 *Trends Ecol. Evol.* **18**, 358-365.

677 Bishop A., Abbott G., 1993. The interrelationship of biological marker maturity parameters and
678 molecular yields during contact-metamorphism. *Geochim. Cosmochim. Acta* **57**, 3661-
679 3668.

680 Bishop A., Love G., McAulay A., Snape C., Farrimond P., 1998. Release of kerogen-bound
681 hopanoids by hydropyrolysis. *Org. Geochem.* **29**, 989-1001.

682 Campbell I., Czamanske G., Fedorenko V., Hill R., Stepanov V., 1992. Synchronism of the
683 Siberian Traps and the Permian-Triassic boundary. *Science* **258**, 1760-1763.

684 Cao C., Love G.D., Hays L., Wang W., Shen S., Summons R.E., 2009. Biogeochemical evidence
685 for euxinic oceans and ecological disturbance presaging the end-Permian mass extinction
686 event. *Earth. Planet. Sci. Lett.* **281**, 188-201.

687 Cao C., Wang W., Jin Y., 2002. Carbon isotope excursions across the Permian-Triassic boundary
688 in the Meishan section, Zhejiang Province, China. *Chinese Sci. Bull.* **47**, 1125-1129.

689 Curiale J., Odermatt J., 1989. Short-term biomarker variability in the Monterey Formation, Santa
690 Maria Basin. *Org. Geochem.* **14**, 1-13.

691 Dahl J., Michael Moldowan J., Sundararaman P., 1993. Relationship of biomarker distribution to
692 depositional environment: Phosphoria Formation, Montana, USA. *Org. Geochem.* **20**,
693 1001-1017.

694 Derenne S., Largeau C., Casadevall E., Connan J., 1988. Comparison of torbanites of various
695 origins and evolutionary stages. Bacterial contribution to their formation. Causes of the
696 lack of botryococcane in bitumens. *Org. Geochem.* **12**, 43-59.

697 Eglinton T., Rowland S., Curtis C., Douglas A., 1986. Kerogen-mineral reactions at raised
698 temperatures in the presence of water. *Org. Geochem.* **10**, 1041-1052.

699 Erwin D.H., 2006. *Extinction: how life on earth nearly ended 250 million years ago*. Princeton
700 University Press.

701 Farrimond P., Griffiths T., Evdokiadis E., 2002. Hopanoic acids in Mesozoic sedimentary rocks:
702 their origin and relationship with hopanes. *Org. Geochem.* **33**, 965-977.

703 Farrimond P., Taylor A., Telnaes N., 1998. Biomarker maturity parameters: the role of generation
704 and thermal degradation. *Org. Geochem.* **29**, 1181-1197.

705 Fritz S., Toth T., 1997. An Fe-berthierine from a Cretaceous laterite. 2. Estimation of Eh, pH and
706 pCO_2 conditions of formation. *Clays Clay Miner.* **45**, 580-586.

707 Grantham P., 1986. Sterane isomerisation and moretane/hopane ratios in crude oils derived from
708 Tertiary source rocks. *Org. Geochem.* **9**, 293-304.

709 Grice K., Cao C., Love G., Bottcher M., Twitchett R., Grosjean E., Summons R., Turgeon S.,
710 Dunning W., Jin Y., 2005. Photic zone euxinia during the Permian-Triassic superanoxic
711 event. *Science* **307**, 706-709.

712 Handley, L., Talbot, H., Cooke, M., Anderson, K., Wagner, T. 2010. Bacteriohopanepolyols as
713 tracers for continental and marine organic matter supply and phases of enhanced nitrogen
714 cycling on the late Quaternary Congo deep sea fan. *Org. Geochem.* **41**, 910-914.

715 Hedges J.I., Keil R.G., 1995. Sedimentary organic matter preservation: an assessment and
716 speculative synthesis. *Mar. Chem.* **49**, 81-115.

717 Huang X., Cui J., Pu Y., Huang J., Blyth A.J., 2008. Identifying "free" and "bound" lipid
718 fractions in stalagmite samples: An example from Heshang Cave, Southern China. *Appl.*
719 *Geochem.* **23**, 2589-2595.

720 Hughes W.B., Dzou L.I.P., 1995. Reservoir overprinting of crude oils. *Org. Geochem.* **23**, 905-
721 914.

722 Huizinga B., Tannenbaum E., Kaplan I., 1987. The role of minerals in the thermal alteration of
723 organic-matter. 4. Generation of normal-alkanes, acyclic isoprenoids, and alkenes in
724 laboratory experiments. *Geochim. Cosmochim. Acta* **51**, 1083-1097.

725 Hveding-Bergseth N., Bruun T., Kjųsen H., 1983. Isolation of 30-nor-21 [alpha]-hopan-22-one
726 (isoadiantone) from the lichen *Platismatia glauca*. *Phytochemistry* **22**, 1826-1827.

727 Isaksen G., Bohacs K., 1995. Geologic controls of source rock geochemistry through relative sea
728 level, in: Katz, B. (Ed.), *Petroleum Source Rocks*. Springer-Verlag, Berlin; New York,
729 pp. 25-50.

730 Ishiwatari R., Yamamoto S., Uemura H., 2005. Lipid and lignin/cutin compounds in Lake Baikal
731 sediments over the last 37 kyr: implications for glacial-interglacial palaeoenvironmental
732 change. *Org. Geochem.* **36**, 327-347.

733 Jaffé R., Diaz D., Hajje N., Chen L., Eckardt C., Furton K.G., 1997. Hydrocarbon speciation in
734 ancient sediments studied by stepwise high-temperature supercritical carbon dioxide
735 extraction. *Org. Geochem.* **26**, 59-65.

736 Jaffé R., Gardinali P., 1990. Generation and maturation of carboxylic acids in ancient sediments
737 from the Maracaibo Basin, Venezuela. *Org. Geochem.* **16**, 211-218.

738 Kaiho K., Chen Z.-Q., Kawahata H., Kajiwara Y., Sato H., 2006. Close-up of the end-Permian
739 mass extinction horizon recorded in the Meishan section, South China: Sedimentary,
740 elemental, and biotic characterization and a negative shift of sulfate sulfur isotope ratio.
741 *Palaeogeogr., Palaeoclimatol., Palaeoecol.* **239**, 396-405.

742 Kaiho K., Kajiwara Y., Nakano T., Miura Y., Kawahata H., Tazaki K., Ueshima M., Chen Z., Shi
743 G., 2001. End-Permian catastrophe by a bolide impact: Evidence of a gigantic release of
744 sulfur from the mantle. *Geology* **29**, 815-818.

745 Kamo S., Czamanske G., Amelin Y., Fedorenko V., Davis D., Trofimov V., 2003. Rapid eruption
746 of Siberian flood-volcanic rocks and evidence for coincidence with the Permian-Triassic
747 boundary and mass extinction at 251 Ma. *Earth. Planet. Sci. Lett.* **214**, 75-91.

748 Kolaczkowska E., Slougui N., Watt D., Maruca R., Michael Moldowan J., 1990. Thermodynamic
749 stability of various alkylated, dealkylated and rearranged 17α-and 17β-hopane isomers
750 using molecular mechanics calculations. *Org. Geochem.* **16**, 1033-1038.

751 Koopmans M., Carson F., Sinninghe Damsté J., Lewan M., 1998. Biomarker generation from
752 Type II-S kerogens in claystone and limestone during hydrous and anhydrous pyrolysis.
753 *Org. Geochem.* **29**, 1395-1402.

754 Kristen I., Wilkes H., Vieth A., Zink K.-G., Plessen B., Thorpe J., Partridge T.C., Oberhaensli H.,
755 2010. Biomarker and stable carbon isotope analyses of sedimentary organic matter from
756 Lake Tswaing: evidence for deglacial wetness and early Holocene drought from South
757 Africa. *J Paleolimnol* **44**, 143-160.

758 Kubicki J., Schroeter L., Itoh M., Nguyen B., Apitz S., 1999. Attenuated total reflectance Fourier-
759 transform infrared spectroscopy of carboxylic acids adsorbed onto mineral surfaces.
760 *Geochim. Cosmochim. Acta* **63**, 2709-2725.

761 Larcher A., Alexander R., Kagi R., 1987. Changes in configuration of extended moretanes with
762 increasing sediment maturity. *Org. Geochem.* **11**, 59-63.

763 Larcher A., Alexander R., Kagi R., 1988. Differences in reactivities of sedimentary hopane
764 diastereomers when heated in the presence of clays. *Org. Geochem.* **13**, 665-669.

765 Lavie D., Jain T., Mahendra K., 1968. Terpenoids--VII. Constituents of *Euphorbia lateriflora*
766 *Schum.* and *Thonn. Phytochemistry* **7**, 657-660.

767 Lockhart R.S., Meredith W., Love G.D., Snape C.E., 2008. Release of bound aliphatic
768 biomarkers via hydropyrolysis from Type II kerogen at high maturity. *Org. Geochem.* **39**,
769 1119-1124.

770 Looy C., Twitchett R., Dilcher D., Konijnenburg-Van Cittert J., Visscher H., 2001. Life in the
771 end-Permian dead zone. *Proc. Natl. Acad. Sci. U. S. A.* **98**, 7879-7883.

772 Lu S., Ruth E., Kaplan I., 1989. Pyrolysis of kerogens in the absence and presence of
773 montmorillonite- I. The generation, degradation and isomerization of steranes and
774 triterpanes at 200-Degrees-C and 300-Degrees-C. *Org. Geochem.* **14**, 491-499.

775 McKirdy D., Aldridge A., Ypma P., 1983. A geochemical comparison of some crude oils from
776 Pre-Ordivician carbonate rocks, in: Bjoroy, M. (Ed.), *Advances in Organic Geochemistry*.
777 John Wiley and Sons, New York, pp. 99-107.

778 Mead R.N., Goni M.A., 2008. Matrix protected organic matter in a river dominated margin: A
779 possible mechanism to sequester terrestrial organic matter? *Geochim. Cosmochim. Acta*
780 **72**, 2673-2686.

781 Metcalfe I., Isozaki Y., 2009. Current perspectives on the Permian–Triassic boundary and end-
782 Permian mass extinction: Preface. *J. Asian Earth Sci.* **36**, 407-412.

783 Michaelsen P., 2002. Mass extinction of peat-forming plants and the effect on fluvial styles
784 across the Permian-Triassic boundary, northern Bowen Basin, Australia. *Palaeogeogr.,*
785 *Palaeoclimatol., Palaeoecol.* **179**, 173-188.

786 Moldowan J., Sundararaman P., Schoell M., 1986. Sensitivity of biomarker properties to
787 depositional environment and/or source input in the Lower Toarcian of SW-Germany.
788 *Org. Geochem.* **10**, 915-926.

789 Mundil R., Ludwig K., Metcalfe I., Renne P., 2004. Age and timing of the Permian mass
790 extinctions: U/Pb dating of closed-system zircons. *Science* **305**, 1760-1763.

Mundil R., Metcalfe I., Ludwig K.R., Renne P.R., Oberli F., Nicoll R.S., 2001. Timing of the Permian-Triassic biotic crisis: implications from new zircon U/Pb age data (and their limitations). *Earth. Planet. Sci. Lett.* **187**, 131-145.

Murray I., Love G., Snape C., Bailey N., 1998. Comparison of covalently-bound aliphatic biomarkers released via hydropyrolysis with their solvent-extractable counterparts for a suite of Kimmeridge clays. *Org. Geochem.* **29**, 1487-1505.

Nabbefeld B., Grice K., Schimmelmann A., Summons R.E., Troitzsch U., Twitchett R.J., 2010a. A comparison of thermal maturity parameters between freely extracted hydrocarbons (Bitumen I) and a second extract (Bitumen II) from within the kerogen matrix of Permian and Triassic sedimentary rocks. *Org. Geochem.* **41**, 78-87.

Nabbefeld, B., Grice, K., Summons, R.E., Hays, L.E., Cao, C., 2010b. Significance of polycyclic aromatic hydrocarbons (PAHs) in Permian/Triassic boundary sections. *Appl. Geochem.* **25**, 1374-1382.

Ourisson G., Albrecht P., 1992. Hopanoids. 1. Geohopanoids - The most abundant natural-products on earth. *Acc. Chem. Res.* **25**, 398-402.

Pan C., Feng J., Tian Y., Yu L., Luo X., Sheng G., Fu J., 2005. Interaction of oil components and clay minerals in reservoir sandstones. *Org. Geochem.* **36**, 633-654.

Pan C., Geng A., Zhong N., Liu J., 2010. Kerogen pyrolysis in the presence and absence of water and minerals: steranes and triterpenoids. *Fuel* **89**, 336-345.

Pan C., Geng A., Zhong N., Liu J., Yu L., 2009. Kerogen pyrolysis in the presence and absence of water and minerals: Amounts and compositions of bitumen and liquid hydrocarbons. *Fuel* **88**, 909-919.

Peters K., Moldowan J., 1991. Effects of source, thermal maturity, and biodegradation on the distribution and isomerization of homohopanes in petroleum. *Org. Geochem.* **17**, 47-61.

Peters K., Moldowan J., Sundararaman P., 1990. Effects of hydrous pyrolysis on biomarker thermal maturity parameters: Monterey phosphatic and siliceous members. *Org. Geochem.* **15**, 249-265.

Peters K.E., Walters C.C., Moldowan J.M., 2005. *The biomarker guide*, 2nd ed. Cambridge University Press, Cambridge, UK ; New York.

Pollastro R.M., 1993. Considerations and applications of the illite/smectite geothermometer in hydrocarbon-bearing rocks of Miocene to Mississippian age. *Clays Clay Miner.* **41**, 119-133.

Quirk M., Wardroper A., Wheatley R., Maxwell J., 1984. Extended hopanoids in peat environments. *Chem. Geol.* **42**, 25-43.

Ransom B., Kim D., Kastner M., Wainwright S., 1998. Organic matter preservation on continental slopes: importance of mineralogy and surface area. *Geochim. Cosmochim. Acta* **62**, 1329-1345.

Raup D., 1979. Size of the Permo-Triassic bottleneck and its evolutionary implications. *Science* **206**, 217-218.

Renne P., Black M., Zichao Z., Richards M., Basu A., 1995. Synchrony and causal relations between Permian-Triassic boundary crises and Siberian flood volcanism. *Science* **269**, 1413-1416.

Retallack G., 1995. Permian-Triassic life crisis on land. *Science* **267**, 77-80.

Retallack G., Seyedolali A., Krull E., Holser W., Ambers C., Kyte F., 1998. Search for evidence of impact at the Permian-Triassic boundary in Antarctica and Australia. *Geology* **26**, 979-982.

Retallack, G., 2005. Earliest Triassic claystone breccias and soil-erosion crisis. *Journal of Sedimentary Research*. **75**. 679-695.

Reynolds Jr. R., Reynolds R., 1996. NEWMOD for windows. The calculations of one dimensional x-ray diffraction patterns of mixed-layered clay minerals, Hanover, NH.

Rosa‐Putra S., Nalin R., Domenach A., Rohmer M., 2001. Novel hopanoids from *Frankia spp.* and related soil bacteria. *Eur. J. Biochem.* **268**, 4300-4306.

Rullkötter J., Marzi R., 1988. Natural and artificial maturation of biological markers in a Toarcian shale from northern Germany. *Org. Geochem.* **13**, 639-645.

Rullkötter J., Spiro B., Nissenbaum A., 1985. Biological marker characteristics of oils and asphalts from carbonate source rocks in a rapidly subsiding graben, Dead Sea, Israel. *Geochim. Cosmochim. Acta* **49**, 1357-1370.

848 Sáenz, J., Eglinton, T., Summons, R., 2011. Abundance and structural diversity of
849 bacteriohopanepolyols in suspended particulate matter along a river ocean transect. *Org*.
850 *Geochem*.**42**, 774-780.

851 Saxby J., Chatfield P., Taylor G., Fitzgerald J., Kaplan I., Lu S., 1992. Effect of clay minerals on
852 products from coal maturation. *Org. Geochem.* **18**, 373-383.

853 Seifert W., Moldowan J., 1980. The effect of thermal stress on source-rock quality as measured
854 by hopane stereochemistry. *Phys Chem Earth* **12**, 229-237.

855 Seifert W., Moldowan M., 1978. Applications of steranes, terpanes and monoaromatics to the
856 maturation, migration and source of crude oils. *Geochim. Cosmochim. Acta* **42**, 77-95.

857 Sephton M.A., Looy C.V., Brinkhuis H., Wignall P.B., De Leeuw J.W., Visscher H., 2005.
858 Catastrophic soil erosion during the end-Permian biotic crisis. *Geology* **33**, 941-944.

859 Sepkoski J.J., 2002. A compendium of fossil marine animal genera. *Bull. Am. Paleontol*. **363**. 1-
860 563.

861 Sheldon, N. D., Retallack, G. J., 2002. Low oxygen levels in earliest Triassic. *Geology*. **30**. 919-
862 922.

863 Shen J., Huang W., 2007. Biomarker distributions as maturity indicators in coals, coaly shales,
864 and shales from Taiwan. *Terr Atmos Ocean Sci* **18**, 739-755.

865 Shen S., Crowley, J.,,Wang, Y., Bowring S., Erwin, D., Sadler, P., Cao C., Rothman, D.,
866 Henderson, C., Ramezani, J., Zhang, H., Shen, Y., Wang, X., Wang, W., Mu, L, Li, W.,

867 Tang, Y., Liu, X., Liu, L., Zeng, Y., Jiang, Y., Jin, Y., 2011. Calibrating the End-Permian
868 Mass Extinction. *Science*, 17 November 2011 (10.1126/science.1213454).

869 Shen, W., Sun, Y., Lin, Y., Liu, D., Chai, P., 2011. Evidence of wildfire in the Meishan section
870 and implications for Permina-Triassic events. *Geochim. Cosmochim. Acta* **75**. 1992-2006.

871 Shiojima K., Ageta H., 1990. Fern constituents: two new triterpenoid hydrocarbons, hop-16-ene
872 and isohop-22(29)-ene, isolated from *Davallia-mariiesii*. *Chem Pharm Bull* **38**, 347-349.

873 Sieskind O., Joly G., Albrecht P., 1979. Simulation of the geochemical transformations of sterols
874 - superacid effect of clay-minerals. *Geochim. Cosmochim. Acta* **43**, 1675-1679.

875 Solomon D., Swift J., 1967. Reactions catalyzed by minerals. Part II. chain termination in free-
876 radical polymerizations. *J. Appl. Polym. Sci.* **11**, 2567-2575.

877 Srodon J., Drits V., McCarty D., Hsieh J., Eberl D., 2001. Quantitative X-ray diffraction analysis
878 of clay-bearing rocks from random preparations. *Clays Clay Miner.* **49**, 514-528.

879 Tannenbaum E., Ruth E., Kaplan I., 1986. Steranes and triterpanes generated from kerogen
880 pyrolysis in the absence and presence of minerals. *Geochim. Cosmochim. Acta* **50**, 805-
881 812.

882 Taylor K., Curtis C., 1995. Stability and facies association of early diagenetic mineral
883 assemblages; an example from a Jurassic ironstone-mudstone succession, UK. *J.*
884 *Sediment Res.* **A65**, 358-368.

885 Thomas M., Clouse J., Longo J., 1993. Adsorption of organic compounds on carbonate minerals.
886 1. Model compounds and their influence on mineral wettability. *Chem. Geol.* **109**, 201-
887 213.

888 Tsuzuki K., Ohashi A., Arai Y., Masuda K., Takano A., Shiojima K., Ageta H., Cai S., 2001.
889 Triterpenoids from *Adiantum caudatum*. *Phytochemistry* **58**, 363-367.

890 Twitchett R., Looy C., Morante R., Visscher H., Wignall P., 2001. Rapid and synchronous
891 collapse of marine and terrestrial ecosystems during the end-Permian biotic crisis.
892 *Geology* **29**, 351-354.

893 Uemura H., Ishiwatari R., 1995. Identification of unusual 17 [beta](H)-moret-22 (29)-ene in lake
894 sediments. *Org. Geochem.* **23**, 675-680.

895 van Kaam-Peters H.M.E., Köster J., van der Gaast S.J., Dekker M., de Leeuw J.W., Sinninghe
896 Damsté J.S., 1998. The effect of clay minerals on diasterane/sterane ratios. *Geochim.*
897 *Cosmochim. Acta* **62**, 2923-2929.

898 Wang C., 2007. Anomalous hopane distributions at the Permian-Triassic boundary, Meishan,
899 China-Evidence for the end-Permian marine ecosystem collapse. *Org. Geochem.* **38**, 52-
900 66.

901 Wang, C., Visscher, H., 2007. Abundance anomalies of aromatic biomarkers in the Permian-
902 Triassic boundary section at Meishan, China - Evidence of end-Permian terrestrial
903 ecosystem collapse.*Palaeogeogr. Palaeoclimatol., Palaeoecol.* **252**, 291-303.

Wang C., Liu Y., Liu H., Zhu L., Shi Q., 2005. Geochemical significance of the relative enrichment of pristane and the negative excursion of delta C-13(Pr) across the Permian-Mriassic Boundary at Meishan, China. *Chinese Sci Bull* **50**, 2213-2225.

Waples D., Machihara T., 1990. Applications of sterane and triterpane biomarkers in petroleum exploration. *Bulletin Canadian Petroleum Geology* **38**, 357-380.

Ward, P.D., Montgomery, D.R., Smith, R., 2000. Altered river morphology in South Africa related to the Permian-Triassic Extinction. **289**, 1740-1743.

Wei Z., Moldowan J., Paytan A., 2006. Diamondoids and molecular biomarkers generated from modern sediments in the absence and presence of minerals during hydrous pyrolysis. *Org. Geochem.* **37**, 891-911.

Wignall P., Hallam A., 1992. Anoxia as a cause of the Permian/Triassic mass extinction: facies evidence from northern Italy and the western United States. *Palaeogeogr., Palaeoclimatol., Palaeoecol.* **93**, 21-46.

Xie S., Pancost R., Huang J., Wignall P., Yu J., Tang X., Chen L., Huang X., Lai X., 2007. Changes in the global carbon cycle occurred as two episodes during the Permian-Triassic crisis. *Geology* **35**, 1083-1086.

Xie S., Pancost R., Yin H., Wang H., Evershed R., 2005. Two episodes of microbial change coupled with Permo/Triassic faunal mass extinction. *Nature* **434**, 494-497.

Table Descriptions

Table 1. Summary of geochemical data

Table 2. Bulk lithology

Table 3. Absolute and relative clay type percentages

Figure Captions

Figure. 1. Structures of the ββ-hopanoid (1), αβ-hopanoid (2), βα-hopanoid (3), and the αα-hopanoid (4) series are illustrated. Key asymmetric carbon atoms of interest are labeled. The mass spectrometry fragment A is marked with the expected mass units depending on methylation. The molecular ion is indicated and has an expected mass of 412 for C_{30} hopane up to 482 for C_{35} hopanes.

Figure 2. Multiple reaction monitoring (MRM) chromatograms from sample MS-core1-35-1 at 94.53 m depth are shown. The MRM transitions are written to the right of the chromatogram. In the left column, the 191.179 fragment corresponds to the A/B rings for homohopanes (see Fig. 1). In the right column, the 205 mass fragment corresponds to the A/B ring fragment for 2α- and 3β-methylhomohopanes. All peaks are marked numerically with the corresponding identification to the right.

Figure 3. Vertical profiles of molecular parameters, including the moretane/hopane ratio (βα/(βα+αβ)) of C_{30} (A), the homohopane series (B), the 2α- and 3β-methylhomohopanes (C), Ts/(Ts+Tm) (D), the C_{35} homohopane index (%) (E), and hopane/sterane (%) (F), are

Comment [KF23]: The color and shadows were removed from the strat column for Fig3-5

Comment [KF24]: These two indicators were added

plotted versus the stratigraphic column (modified from Cao et al., 2009). The Ts/Ts+Tm, C_{35} HHI, and hopane/sterane data are from Cao et al., 2009. The three moretane/hopane excursions occur at 39.56 m, 92.61-102.59 m, and 186.91-213.52 m. The legend for the stratigraphic column is at bottom right. In the expanded view of the conodont zones in the legend, the PTB is marked according to the first appearance of the conodont *Hindeodus parvus*, and the extinction horizon (EH) is marked at the top of bed 24.

Comment [KF25]: The location of the 3 moretane anomalies were specified as suggested by Ken.

Comment [KF26]: The locations of the PTB and extinction horizon were clarified next to the legend as a result of Ken's comment

Figure 4. Vertical profiles of the bulk lithological components by percentage versus the stratigraphic column (modified from Cao et al., 2009). A) percentage carbonate; B) percentage total clay; C) percentage quartz.

Figure 5. Vertical profiles of clay types plotted against the stratigraphic column (modified from Cao et al. 2009). A) Absolute percent illite; B) absolute percent chlorite; C) absolute percent smectite; D) absolute percent kaolinite; E) absolute percent mixed layer illite/smectite (I/S); F) absolute percent berthierine. Note the difference in the x axis scale for clay types.

Figure 6. Cross-correlations of molecular indicies. Plots A and B relate moretane/hopane of the C_{30} hopane to the higher homologues of the homohopane series and 2α- & 3β-methylhomohopane series, respectively. Plots C and D relate Ts /(Ts+Tm) to the higher homologues of the homohopane series and 2α- and 3β-methylhomohopane series, respectively. The R^2 value associated with the linear regression for each series relationship is given in the legend.

Figure 7. Cross-correlations of molecular and bulk lithological data. Plots A and B relate carbonate weight percentage and total bulk clay to the homohopane series, respectively. Plots C and D relate carbonate weight percentage and total bulk clay to the 2α- and 3β-methylhomohopane series. Plots E and F relate carbonate weight percentage and total bulk clay to Ts/(Ts+Tm).

Figure 8. Correlations between moretane/hopane ratios and the specific clay types are shown for the homohopane and 2α- and 3β-methylhomohopane series. The R^2 values are listed in the legend next to the corresponding series. A) Percent chlorite; B) percent illite; C) percent mixed layer illite/smectite (I/S); D) percent smectite; E) percent kaolinite.

Figure 9. Correlations of geochemical source and redox indicators against moretane/hopane ratios and Ts/(Ts+Tm). C_{35} HHI (%) vs. homohopanes βα/(βα+αβ) (A), methylhomohopanes βα/(βα+αβ) (C), and Ts/(Ts+Tm) (E). Hopane/Sterane (%) versus homohopanes βα/(βα+αβ) (B), methylhomohopanes βα/(βα+αβ) (D), and Ts/(Ts+Tm) (F).

Figure 10. Correlations of geochemical source and redox indicators against percent total clay and clay types. C_{35} HHI (%) vs. percent total clay (A), absolute percent chlorite (C), absolute percent illite (E), absolute percent illite/smectite mixed layer clay (I/S) (G), absolute percent smectite (I), absolute percent kaolinite (K), absolute percent berthierine (M). Hopane/Sterane (%) vs. percent total clay (B), absolute percent chlorite (D),

absolute percent illite (F), absolute percent illite/smectite mixed layer clay (I/S) (H), absolute percent smectite (J), absolute percent kaolinite (L), absolute percent berthierine (N).

Comment [KF27]: Two new figures were prepared to illustrate the new relationships we noticed as a result of the reviewers suggestions

Table 1

Sample ID	Drilling Depth (m)	C_{30} βα/(βα+αβ)	C_{31} βα/(βα+αβ)	C_{32} βα/(βα+αβ)	C_{33} βα/(βα+αβ)	C_{34} βα/(βα+αβ)	2α Me C_{31} βα/(βα+αβ)	2α Me C_{32} βα/(βα+αβ)	2α Me C_{33} βα/(βα+αβ)	3β Me C_{33} βα/(βα+αβ)
MS05-140	7.05	0.069	0.101	0.067	0.075	0.080	0.070	0.104	0.037	0.103
MS05-165	31.05	0.059	0.092	0.060	0.074	0.043	0.045	0.111	-	-
MS05-170	39.56	0.138	0.151	0.122	0.129	0.133	0.135	0.142	0.112	0.140
MS05-175	46.79	0.060	0.098	0.041	0.054	0.063	0.047	0.092	-	-
MS05-180	61.77	0.118	0.135	0.103	0.098	0.088	0.091	0.151	0.098	0.113
MS05-200	89.71	0.152	0.140	0.140	0.145	0.134	0.154	0.209	0.132	0.189
MS-1-core 36-3	92.61	0.335	0.223	0.227	0.267	0.246	0.302	0.304	0.244	0.260
MS-1-core 35-1	94.53	0.343	0.228	0.233	0.267	0.221	0.329	0.290	0.238	0.234
MS-1-core 34-3	102.59	0.300	0.197	0.210	0.222	0.226	0.298	0.263	-	0.205
MS05-2b	111.44	0.053	0.043	0.036	0.075	0.070	0.064	0.078	-	-
MS05-10	116.51	0.048	0.088	0.041	0.050	0.090	0.075	0.087	0.052	0.068
MS05-30	127.82	0.048	0.103	0.057	0.055	0.048	0.084	0.102	0.056	0.062
MS05-60	147.08	0.045	0.092	0.035	0.043	0.041	0.055	0.088	0.030	0.121
MS05-76	157.48	0.052	0.085	0.039	0.053	0.044	0.063	0.083	0.045	0.045
MS05-92b	169.24	0.045	0.084	0.044	0.052	0.046	0.046	0.079	0.056	0.067
MS05-117	186.91	0.211	0.172	0.168	0.176	0.168	0.208	0.227	0.193	0.177
MS05-134	208.22	0.222	0.170	0.175	0.180	0.163	0.271	0.251	0.200	0.165
MS05-136c	211.3	0.188	0.161	0.146	0.165	0.155	0.190	0.226	0.220	0.157
MS05-138	213.52	0.073	0.090	0.057	0.066	0.051	0.080	0.088	0.054	0.093

Table 2

Sample ID	*Percent Clay*	*Percent Carbonate*	*Percent Quartz*	*Percent Other*
MS05-140	0.12	99.03	0.85	0.00
MS05-165	0.16	99.02	0.82	0.00
MS05-170	2.74	96.19	1.07	0.00
MS05-175	2.52	96.61	0.74	0.13
MS05-180	1.37	98.48	0.11	0.04
MS05-200	41.55	14.59	42.76	1.11
MS-1-core 36-3	45.03	20.44	28.13	6.41
MS-1-core 35-1	47.86	16.49	29.28	6.38
MS-1-core 34-3	49.75	14.42	31.43	4.41
MS05-2b	2.01	82.21	15.79	0.00
MS05-10	0.49	90.67	8.84	0.00
MS05-30	6.90	44.46	48.52	0.12
MS05-60	1.83	62.04	36.08	0.05
MS05-76	0.00	77.66	22.35	0.00
MS05-92b	0.27	91.70	8.03	0.00
MS05-117	43.64	8.54	42.81	5.00
MS05-134	26.33	10.32	58.64	4.71
MS05-136c	38.83	11.40	42.84	6.93
MS05-138	2.64	13.76	78.86	4.74

Table 3

Sample ID	*Absolute Percent Illite*	*Absolute Percent Berthierine*	*Absolute Percent Kaolinite*	*Absolute Percent Chlorite*	*Absolute Percent Illite/Smectite Mixed Layer*	*Absolute Percent Smectite*
MS05-140	0.1	0.0	0.0	0.0	0.0	0.0
MS05-165	0.1	0.0	0.1	0.0	0.0	0.0
MS05-170	1.4	0.0	0.0	0.5	0.8	0.0
MS05-175	1.3	0.0	0.0	0.4	0.8	0.0
MS05-180	0.6	0.0	0.0	0.2	0.5	0.0
ms05-200	14.7	0.0	0.3	3.4	13.2	10.0
ms-1-core 36-3	14.5	0.0	0.0	6.9	18.4	5.3
ms-1-core 35-1	17.3	0.0	0.0	9.4	13.9	7.2
ms-1-core 34-3	16.4	0.0	0.0	8.3	15.3	9.7
ms05-2b	0.3	0.0	0.3	0.0	1.5	0.0
MS05-10	0.2	0.0	0.1	0.0	0.2	0.0
MS05-30	0.8	0.0	2.1	0.0	4.0	0.0
MS05-60	0.3	0.0	0.9	0.0	0.6	0.0
MS05-76	0.0	0.0	0.0	0.0	0.0	0.0
MS05-92b	0.1	0.0	0.1	0.0	0.1	0.0
MS05-117	7.4	2.4	7.5	6.2	20.1	0.0
MS05-134	6.3	2.7	4.7	3.6	9.0	0.0
MS05-136c	11.5	3.8	5.4	5.8	12.2	0.0
MS05-138	0.7	0.3	0.0	1.0	0.7	0.0

Sample ID	*Relative Percent Illite*	*Relative Percent Berthierine*	*Relative Percent Kaolinite*	*Relative Percent Chlorite*	*Relative Percent Illite/Smectite Mixed Layer*	*Relative Percent Smectite*
MS05-140	54.4	0.0	10.7	4.4	30.5	0.0
MS05-165	35.8	0.0	37.2	0.0	27.0	0.0
MS05-170	52.9	0.0	0.0	17.4	29.5	0.1
MS05-175	51.7	0.0	0.3	16.8	31.2	0.0
MS05-180	46.3	0.0	0.0	14.9	38.7	0.1
ms05-200	35.4	0.0	0.7	8.1	31.8	24.0
ms-1-core 36-3	32.3	0.0	0.0	15.3	40.8	11.7
ms-1-core 35-1	36.2	0.0	0.0	19.6	29.1	15.1
ms-1-core 34-3	33.0	0.0	0.0	16.7	30.7	19.6
ms05-2b	13.0	0.0	12.5	0.0	74.4	0.0
MS05-10	51.0	0.0	13.3	0.0	35.7	0.0
MS05-30	11.0	0.0	31.0	0.0	58.0	0.0
MS05-60	15.3	0.0	49.4	0.0	35.2	0.0
MS05-76	48.3	0.0	17.5	0.0	34.1	0.0
MS05-92b	38.6	0.0	20.1	0.0	41.2	0.2
MS05-117	16.9	5.6	17.3	14.2	45.9	0.1
MS05-134	24.1	10.1	18.0	13.5	34.2	0.0
MS05-136c	29.7	9.9	13.9	15.0	31.4	0.1
MS05-138	25.8	11.4	0.4	36.4	26.1	0.0

Figure 1

1.

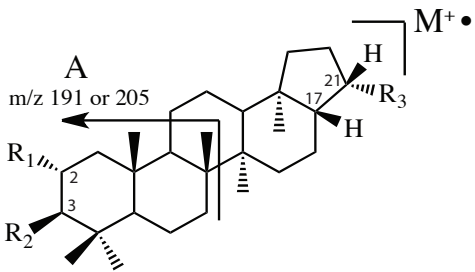

R_1= CH_3, 2α(Me), 17β(H), 21β(H)–hopane; Fragment A m/z=205

R_2= CH_3, 3β(Me), 17β(H), 21β(H)–hopane; Fragment A m/z=205

R_1= R_2= H, 17β(H), 21β(H)–hopane; Fragment A m/z=191

R_3=  n= 0-5

2.

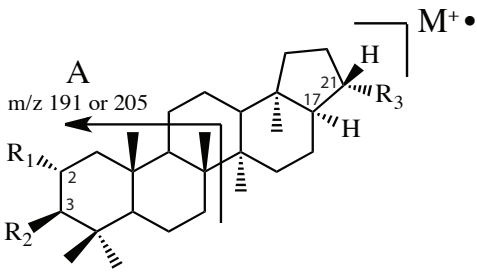

R_1= CH_3, 2α(Me), 17α(H), 21β(H)–hopane; Fragment A m/z=205

R_2= CH_3, 3β(Me), 17α(H), 21β(H)–hopane; Fragment A m/z=205

R_1= R_2= H, 17α(H), 21β(H)–hopane; Fragment A m/z=191

R_3=  n= 0-5

3.

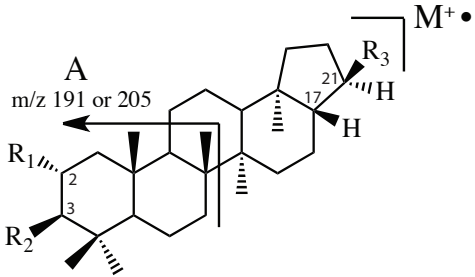

R_1= CH_3, 2α(Me), 17β(H), 21α(H)–hopane; Fragment A m/z=205

R_2= CH_3, 3β(Me), 17β(H), 21α(H)–hopane; Fragment A m/z=205

R_1= R_2= H, 17β(H), 21α(H)–hopane; Fragment A m/z=19

R_3=  n= 0-5

4.

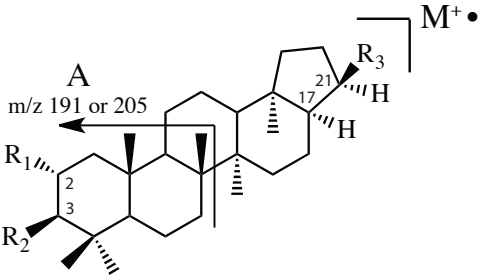

R_1= CH_3, 2α(Me), 17α(H), 21α(H)–hopane; Fragment A m/z=205

R_2= CH_3, 3β(Me), 17α(H), 21α(H)–hopane; Fragment A m/z=205

R_1= R_2= H, 17α(H), 21α(H)–hopane; Fragment A m/z=191

R_3=  n= 0-5

Figure 2

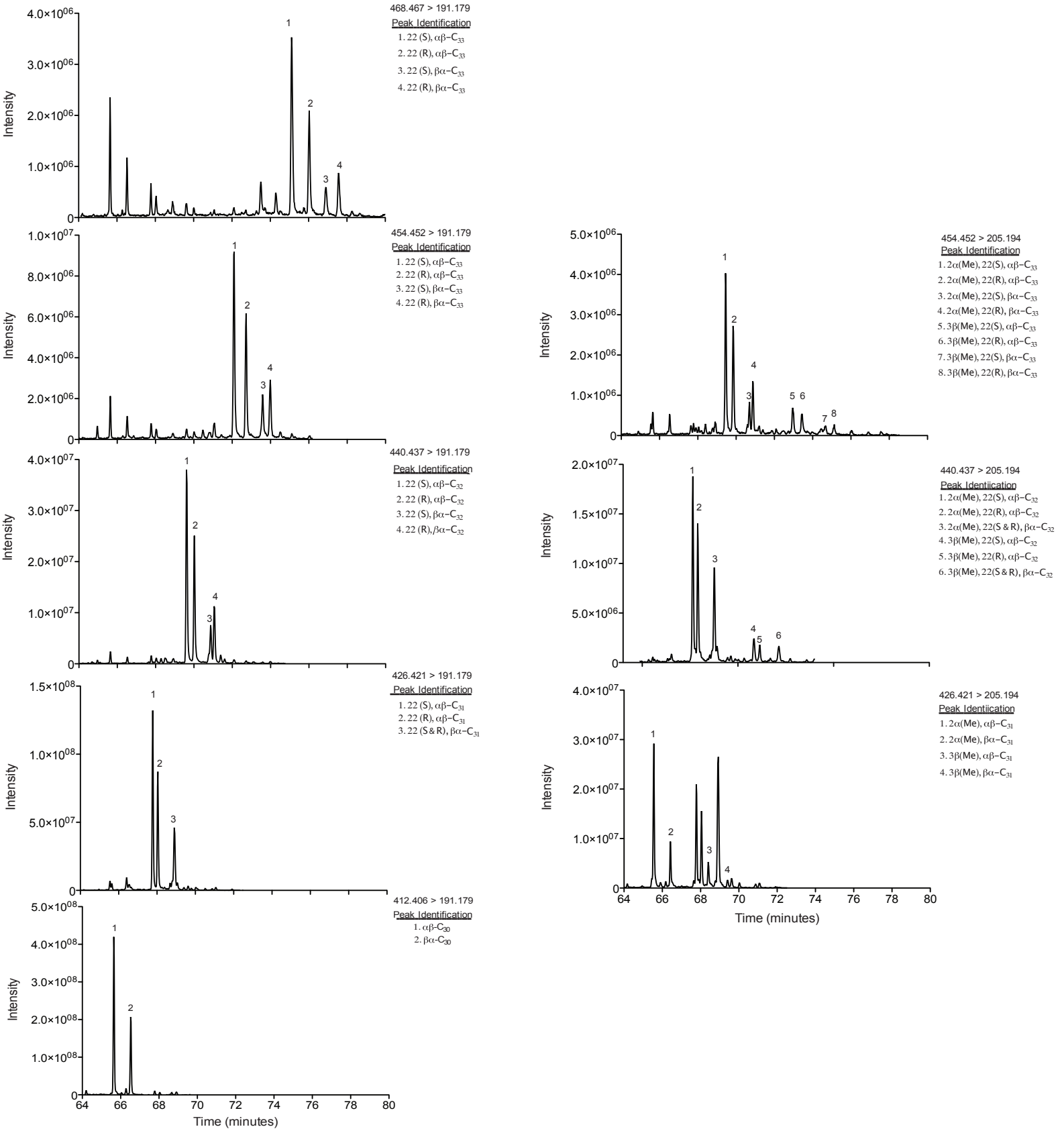
468.467 > 191.179
Peak Identification
1. 22 (S), αβ−C33
2. 22 (R), αβ−C33
3. 22 (S), βα−C33
4. 22 (R), βα−C33
454.452 > 191.179
Peak Identification
1. 22 (S), αβ−C33
2. 22 (R), αβ−C33
3. 22 (S), βα−C33
4. 22 (R), βα−C33
440.437 > 191.179
Peak Identification
1. 22 (S), αβ−C32
2. 22 (R), αβ−C32
3. 22 (S), βα−C32
4. 22 (R), βα−C32
426.421 > 191.179
Peak Identification
1. 22 (S), αβ−C31
2. 22 (R), αβ−C31
3. 22 (S&R), βα−C31
412.406 > 191.179
Peak Identification
1. αβ-C30
2. βα-C30
454.452 > 205.194
Peak Identification
1. 2α(Me), 22(S), αβ−C33
2. 2α(Me), 22(R), αβ−C33
3. 2α(Me), 22(S), βα−C33
4. 2α(Me), 22(R), βα−C33
5. 3β(Me), 22(S), αβ−C33
6. 3β(Me), 22(R), αβ−C33
7. 3β(Me), 22(S), βα−C33
8. 3β(Me), 22(R), βα−C33
440.437 > 205.194
Peak Identiication
1. 2α(Me), 22(S), αβ−C32
2. 2α(Me), 22(R), αβ−C32
3. 2α(Me), 22(S&R), βα−C32
4. 3β(Me), 22(S), αβ−C32
5. 3β(Me), 22(R), αβ−C32
6. 3β(Me), 22(S&R), βα−C32
426.421 > 205.194
Peak Identiication
1. 2α(Me), αβ−C31
2. 2α(Me), βα−C31
3. 3β(Me), αβ−C31
4. 3β(Me), βα−C31
Intensity
Time (minutes)

Figure 3

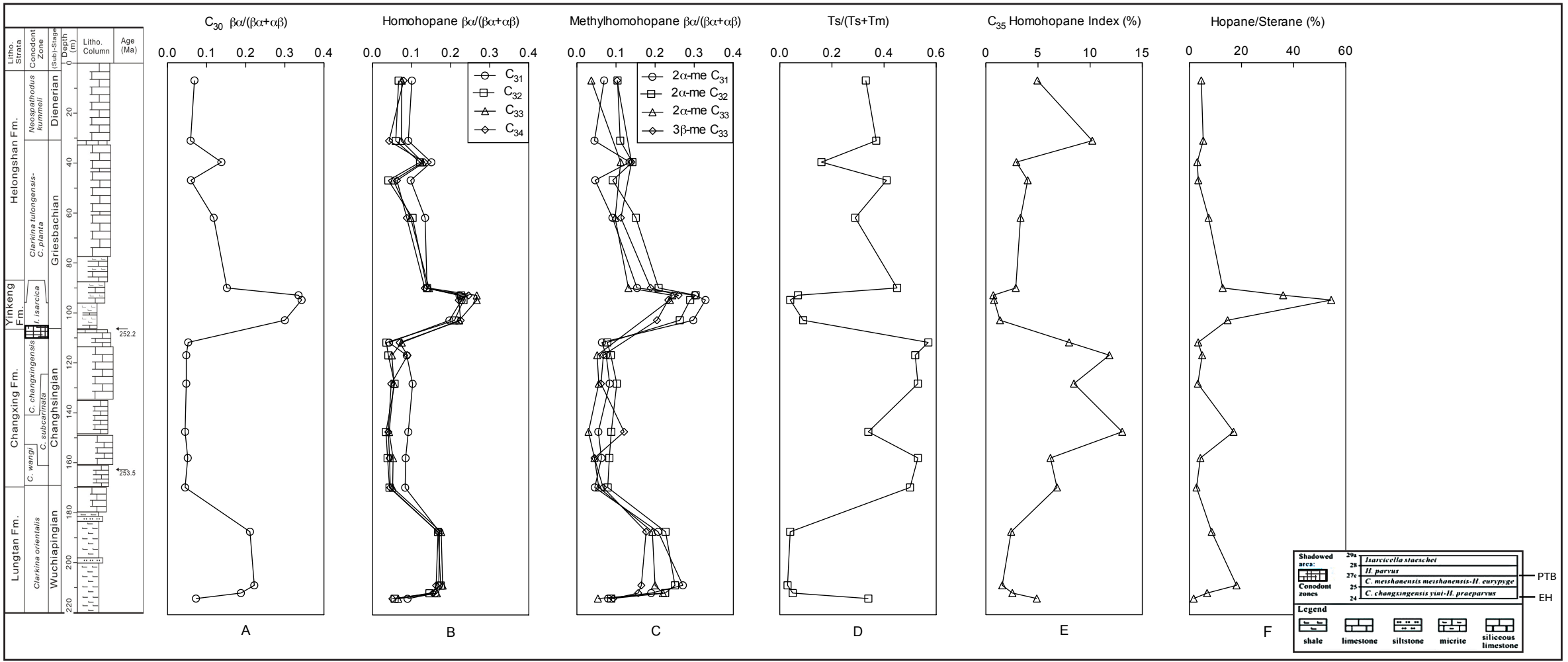
Litho. Strata
Conodont Zone
(Sub)-Stage
Depth (m)
Litho. Column
Age (Ma)
Helongshan Fm.
Yinkeng Fm.
Changxing Fm.
Lungtan Fm.
Neospathodus kummeli
Clarkina tulongensis-C. planta
I. isarcica
C. changxingensis
C. subcarinata
C. wangi
Clarkina orientalis
Dienerian
Griesbachian
Changhsingian
Wuchiapingian
252.2
253.5
C30 βα/(βα+αβ)
Homohopane βα/(βα+αβ)
Methylhomohopane βα/(βα+αβ)
Ts/(Ts+Tm)
C35 Homohopane Index (%)
Hopane/Sterane (%)
C31
C32
C33
C34
2α-me C31
2α-me C32
2α-me C33
3β-me C33
A
B
C
D
E
F
Shadowed area:
Conodont zones
29a
28
27c
25
24
Isarcicella staeschei
H. parvus
C. meishanensis meishanensis-H. eurypyge
C. changxingensis yini-H. praeparvus
PTB
EH
Legend
shale
limestone
siltstone
micrite
siliceous limestone

Figure 4

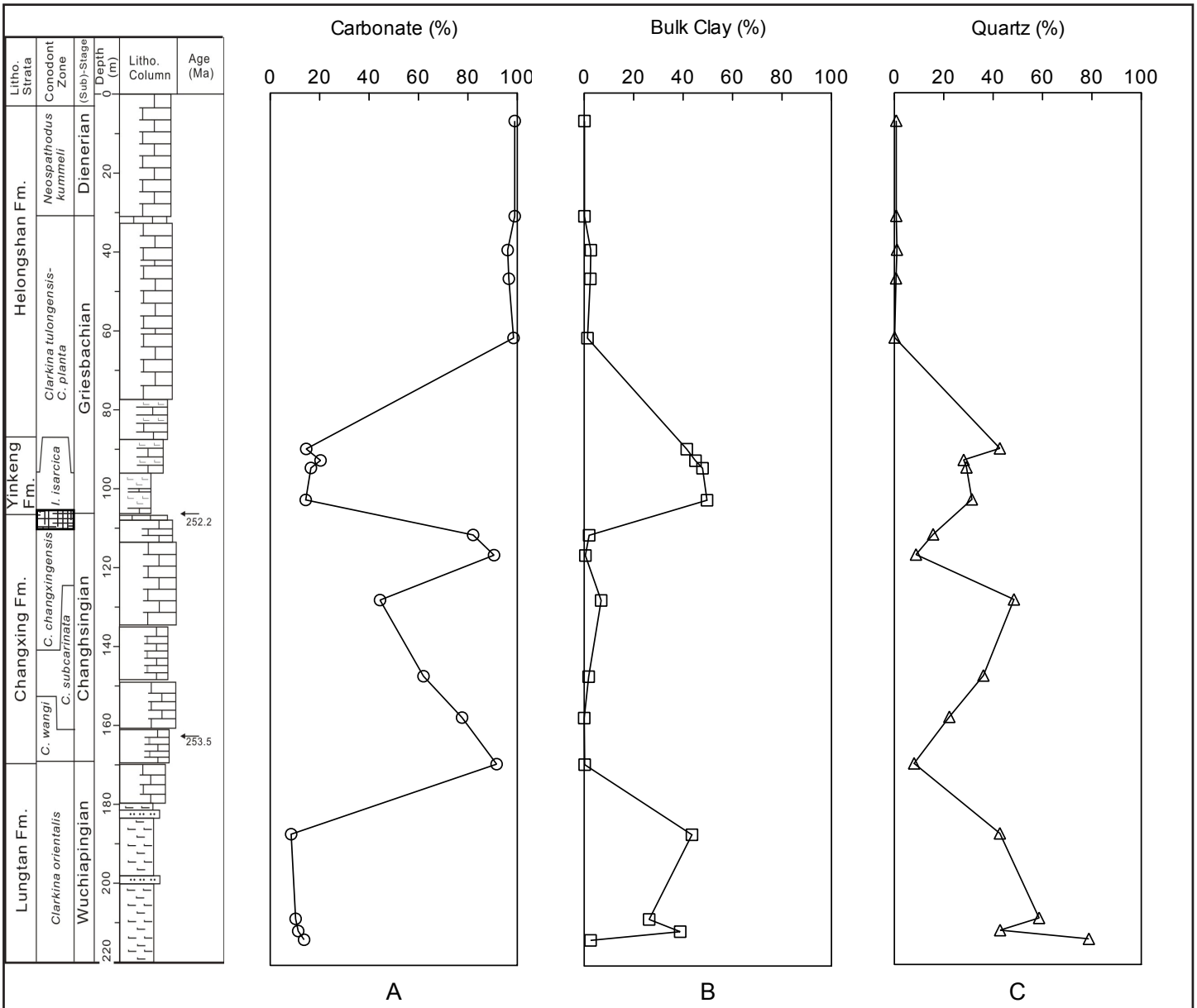
Litho. Strata
Conodont Zone
(Sub)-Stage
Depth (m)
Litho. Column
Age (Ma)
Lungtan Fm.
Changxing Fm.
Yinkeng Fm.
Helongshan Fm.
Clarkina orientalis
C. wangi
C. subcarinata
C. changxingensis
I. isarcica
Clarkina tulongensis-C. planta
Neospathodus kummeli
Wuchiapingian
Changhsingian
Griesbachian
Dienerian
252.2
253.5
Carbonate (%)
Bulk Clay (%)
Quartz (%)
0 20 40 60 80 100
A
B
C

Figure 5

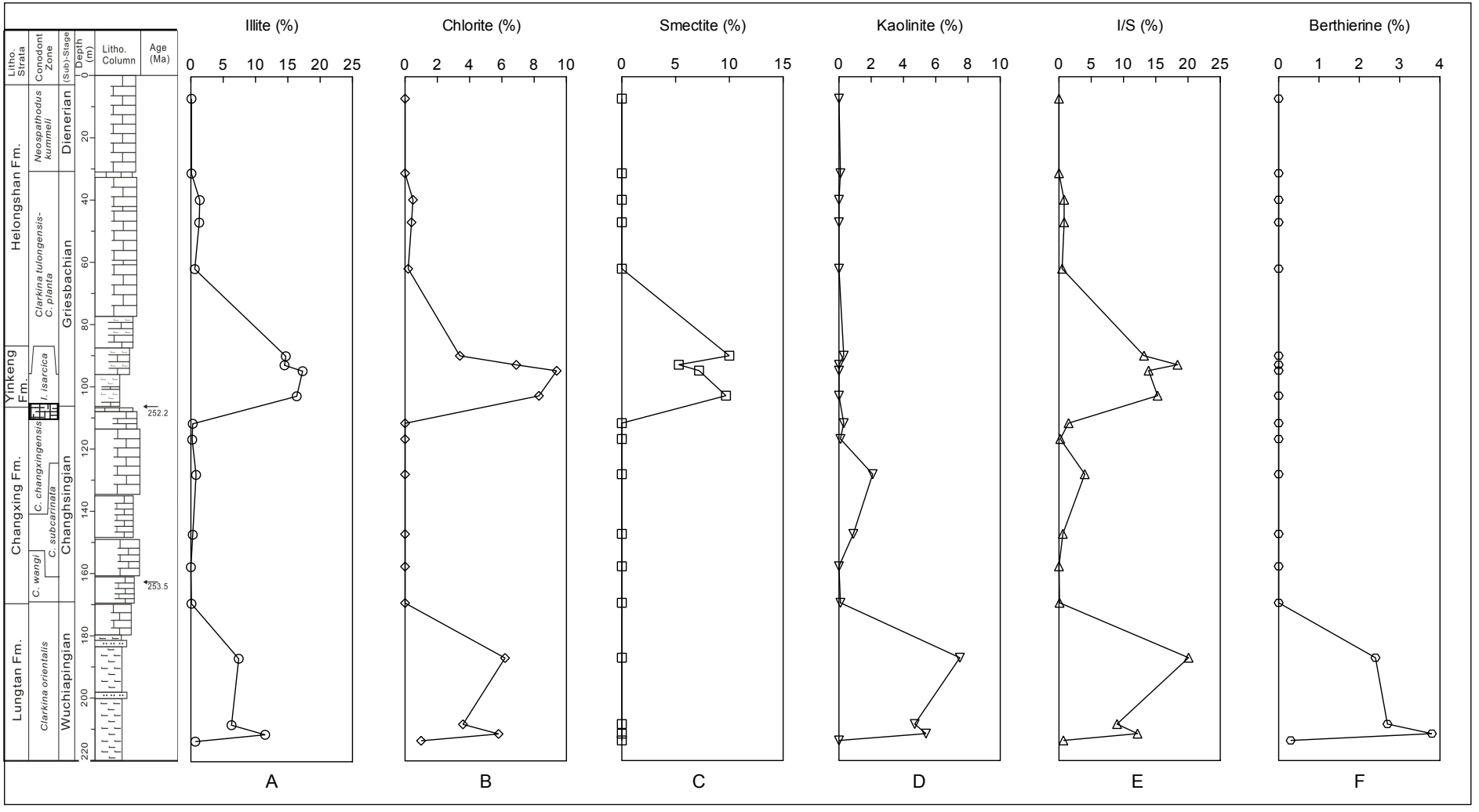
Litho. Strata
Conodont Zone
(Sub)-Stage
Depth (m)
Litho. Column
Age (Ma)
Helongshan Fm.
Yinkeng Fm.
Changxing Fm.
Lungtan Fm.
Neospathodus kummeli
Clarkina tulongensis-C. planta
I. isarcica
C. changxingensis
C. subcarinata
C. wangi
Clarkina orientalis
Dienerian
Griesbachian
Changhsingian
Wuchiapingian
252.2
253.5
Illite (%)
Chlorite (%)
Smectite (%)
Kaolinite (%)
I/S (%)
Berthierine (%)
A
B
C
D
E
F

Figure 6

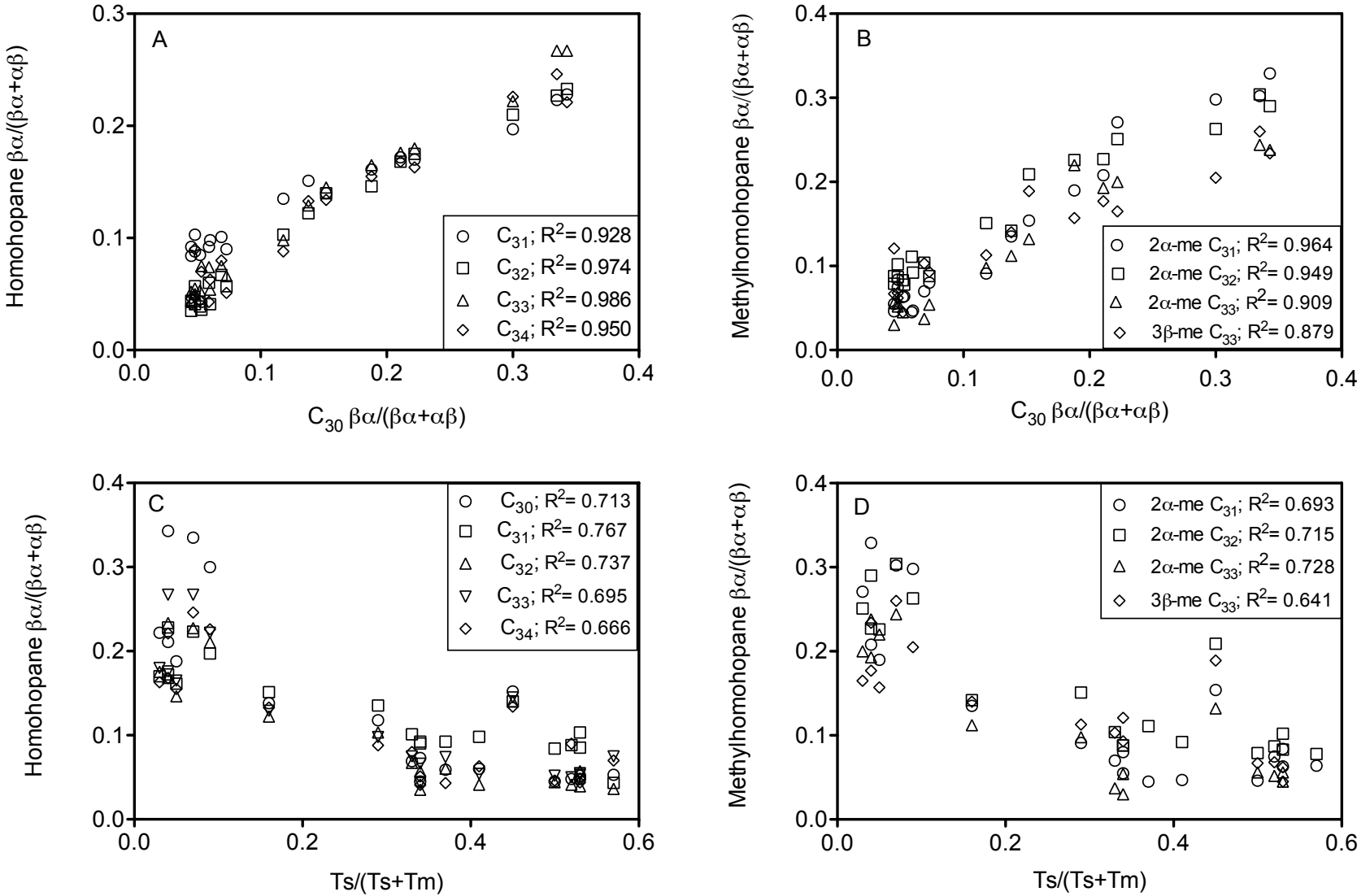
A
Homohopane βα/(βα+αβ)
C30 βα/(βα+αβ)
C31; R2= 0.928
C32; R2= 0.974
C33; R2= 0.986
C34; R2= 0.950
B
Methylhomohopane βα/(βα+αβ)
C30 βα/(βα+αβ)
2α-me C31; R2= 0.964
2α-me C32; R2= 0.949
2α-me C33; R2= 0.909
3β-me C33; R2= 0.879
C
Homohopane βα/(βα+αβ)
Ts/(Ts+Tm)
C30; R2= 0.713
C31; R2= 0.767
C32; R2= 0.737
C33; R2= 0.695
C34; R2= 0.666
D
Methylhomohopane βα/(βα+αβ)
Ts/(Ts+Tm)
2α-me C31; R2= 0.693
2α-me C32; R2= 0.715
2α-me C33; R2= 0.728
3β-me C33; R2= 0.641

Figure 7

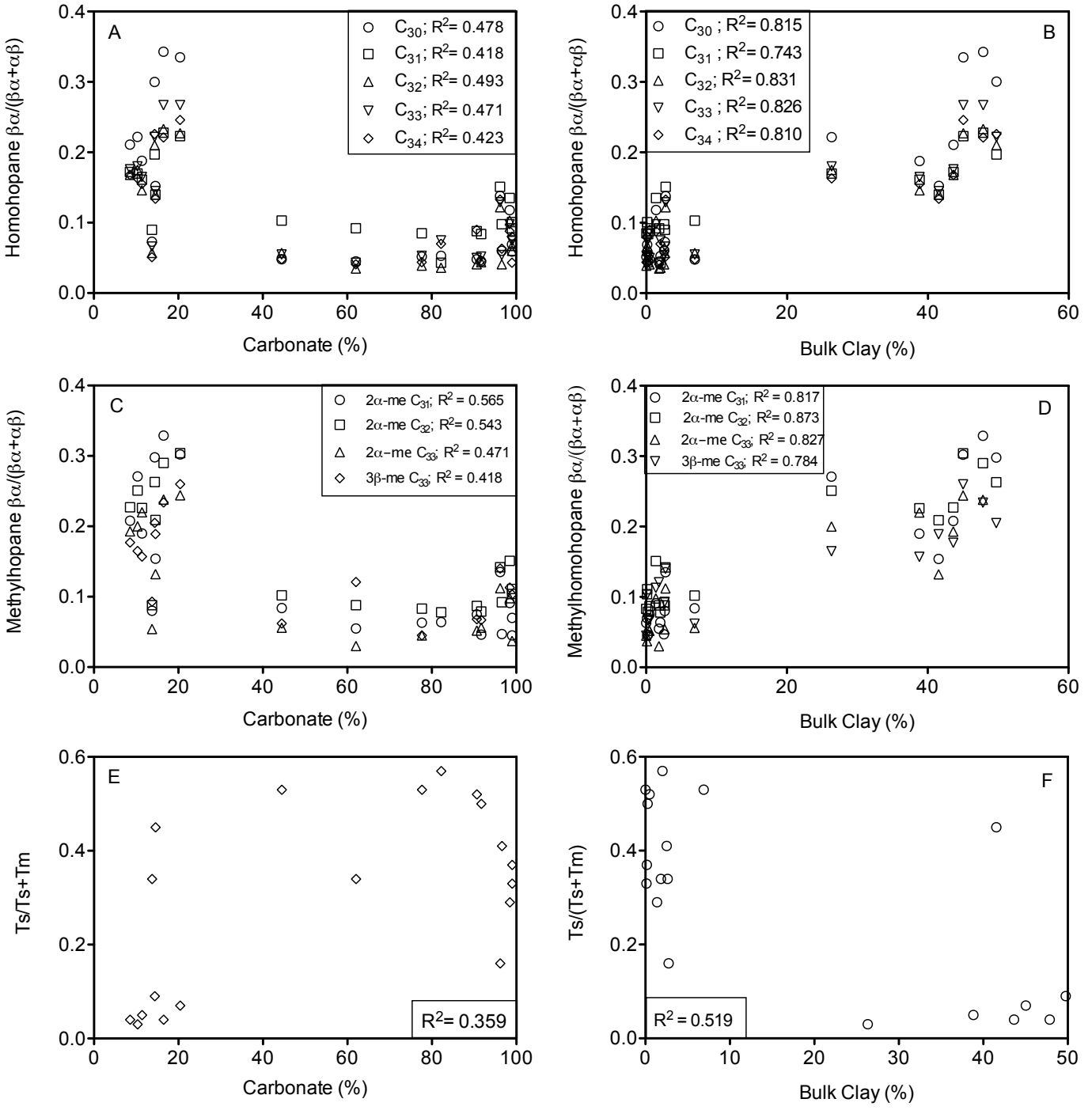
A
B
C
D
E
F
Homohopane βα/(βα+αβ)
Methylhopane βα/(βα+αβ)
Methylhomohopane βα/(βα+αβ)
Ts/Ts+Tm
Ts/(Ts+Tm)
Carbonate (%)
Bulk Clay (%)
C30; R2= 0.478
C31; R2= 0.418
C32; R2= 0.493
C33; R2= 0.471
C34; R2= 0.423
C30 ; R2= 0.815
C31 ; R2= 0.743
C32; R2= 0.831
C33 ; R2= 0.826
C34 ; R2= 0.810
2α-me C31; R2 = 0.565
2α-me C32; R2= 0.543
2α-me C33; R2 = 0.471
3β-me C33; R2 = 0.418
2α-me C31; R2 = 0.817
2α-me C32; R2= 0.873
2α-me C33; R2 = 0.827
3β-me C33; R2 = 0.784
R2= 0.359
R2 = 0.519

Figure 8

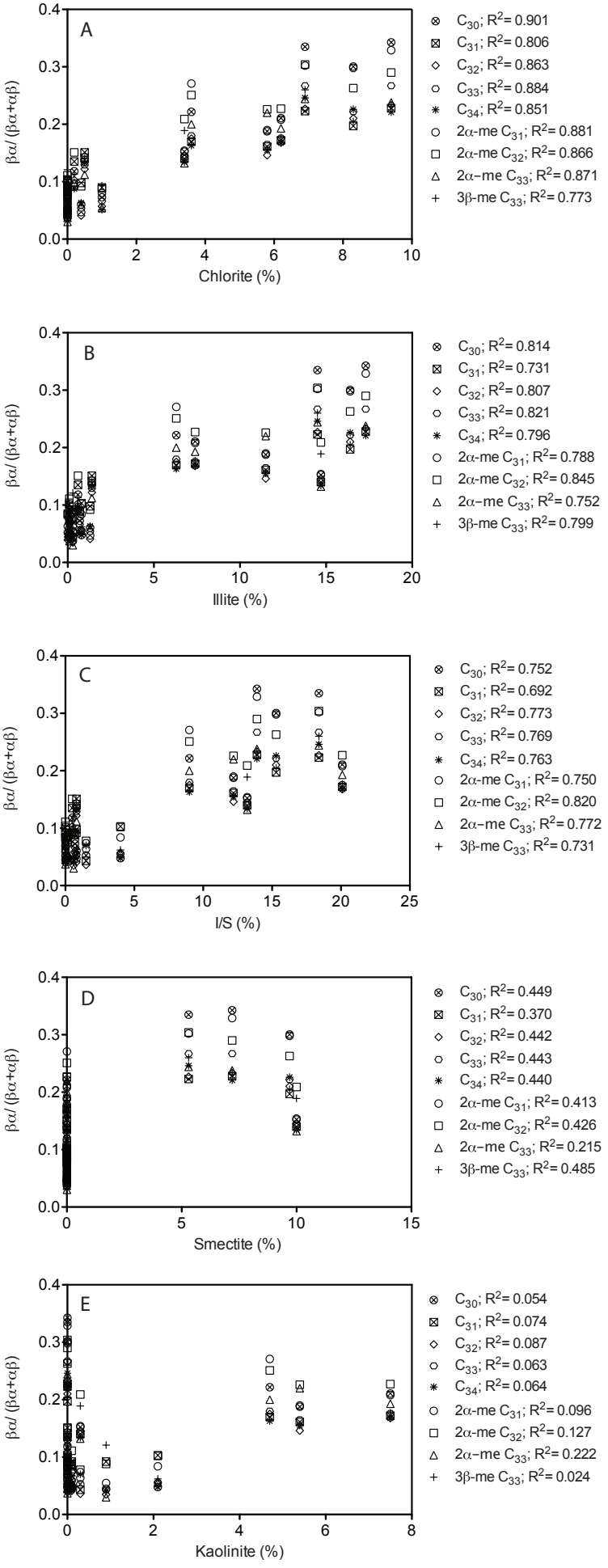
A
βα/ (βα+αβ)
Chlorite (%)
C30; R2= 0.901
C31; R2= 0.806
C32; R2= 0.863
C33; R2= 0.884
C34; R2= 0.851
2α-me C31; R2= 0.881
2α-me C32; R2= 0.866
2α−me C33; R2= 0.871
3β-me C33; R2= 0.773
B
βα/ (βα+αβ)
Illite (%)
C30; R2= 0.814
C31; R2= 0.731
C32; R2= 0.807
C33; R2= 0.821
C34; R2= 0.796
2α-me C31; R2= 0.788
2α-me C32; R2= 0.845
2α−me C33; R2= 0.752
3β-me C33; R2= 0.799
C
βα/ (βα+αβ)
I/S (%)
C30; R2= 0.752
C31; R2= 0.692
C32; R2= 0.773
C33; R2= 0.769
C34; R2= 0.763
2α-me C31; R2= 0.750
2α-me C32; R2= 0.820
2α−me C33; R2= 0.772
3β-me C33; R2= 0.731
D
βα/ (βα+αβ)
Smectite (%)
C30; R2= 0.449
C31; R2= 0.370
C32; R2= 0.442
C33; R2= 0.443
C34; R2= 0.440
2α-me C31; R2= 0.413
2α-me C32; R2= 0.426
2α−me C33; R2= 0.215
3β-me C33; R2= 0.485
E
βα/ (βα+αβ)
Kaolinite (%)
C30; R2= 0.054
C31; R2= 0.074
C32; R2= 0.087
C33; R2= 0.063
C34; R2= 0.064
2α-me C31; R2= 0.096
2α-me C32; R2= 0.127
2α−me C33; R2= 0.222
3β-me C33; R2= 0.024

Figure 9

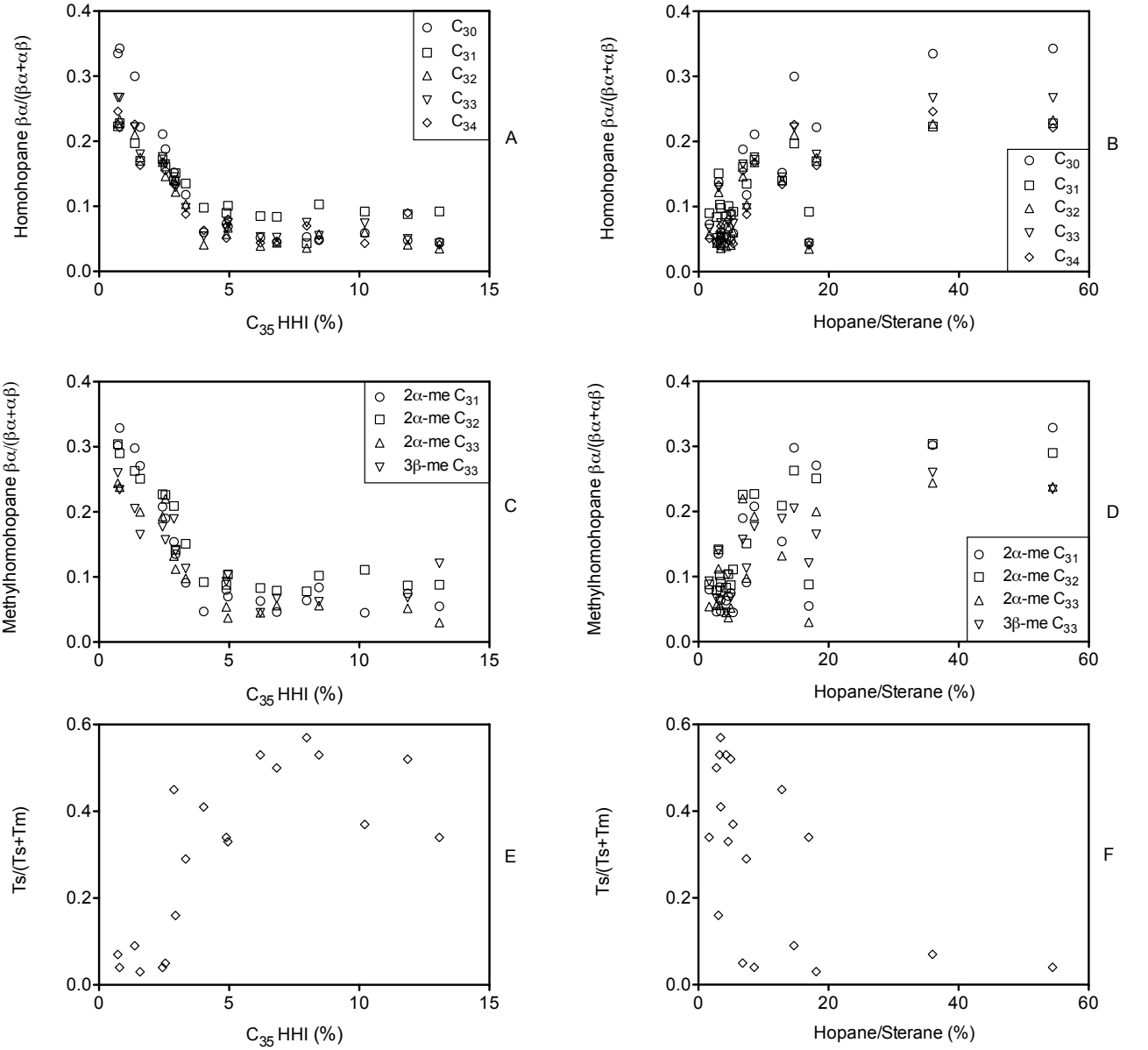
A
Homohopane βα/(βα+αβ)
C35 HHI (%)
C30
C31
C32
C33
C34
B
Homohopane βα/(βα+αβ)
Hopane/Sterane (%)
C30
C31
C32
C33
C34
C
Methylhomohopane βα/(βα+αβ)
C35 HHI (%)
2α-me C31
2α-me C32
2α-me C33
3β-me C33
D
Methylhomohopane βα/(βα+αβ)
Hopane/Sterane (%)
2α-me C31
2α-me C32
2α-me C33
3β-me C33
E
Ts/(Ts+Tm)
C35 HHI (%)
F
Ts/(Ts+Tm)
Hopane/Sterane (%)

Figure 10

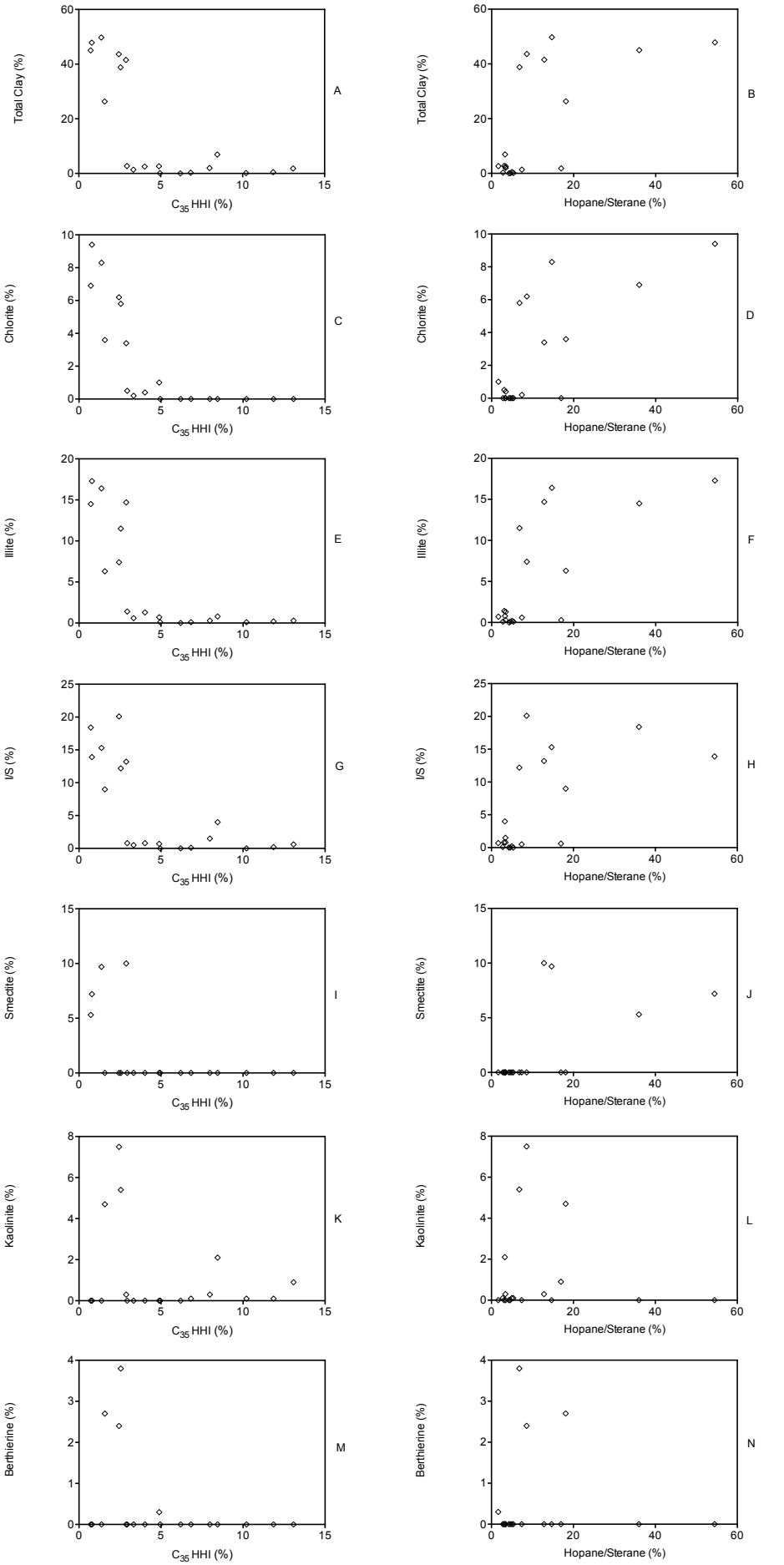
Total Clay (%)
A
C_{35} HHI (%)
Total Clay (%)
B
Hopane/Sterane (%)
Chlorite (%)
C
C_{35} HHI (%)
Chlorite (%)
D
Hopane/Sterane (%)
Illite (%)
E
C_{35} HHI (%)
Illite (%)
F
Hopane/Sterane (%)
I/S (%)
G
C_{35} HHI (%)
I/S (%)
H
Hopane/Sterane (%)
Smectite (%)
I
C_{35} HHI (%)
Smectite (%)
J
Hopane/Sterane (%)
Kaolinite (%)
K
C_{35} HHI (%)
Kaolinite (%)
L
Hopane/Sterane (%)
Berthierine (%)
M
C_{35} HHI (%)
Berthierine (%)
N
Hopane/Sterane (%)